Volume 6
Number 14
21 July 2025
Pages 4553–4926

Materials Advances

rsc.li/materials-advances

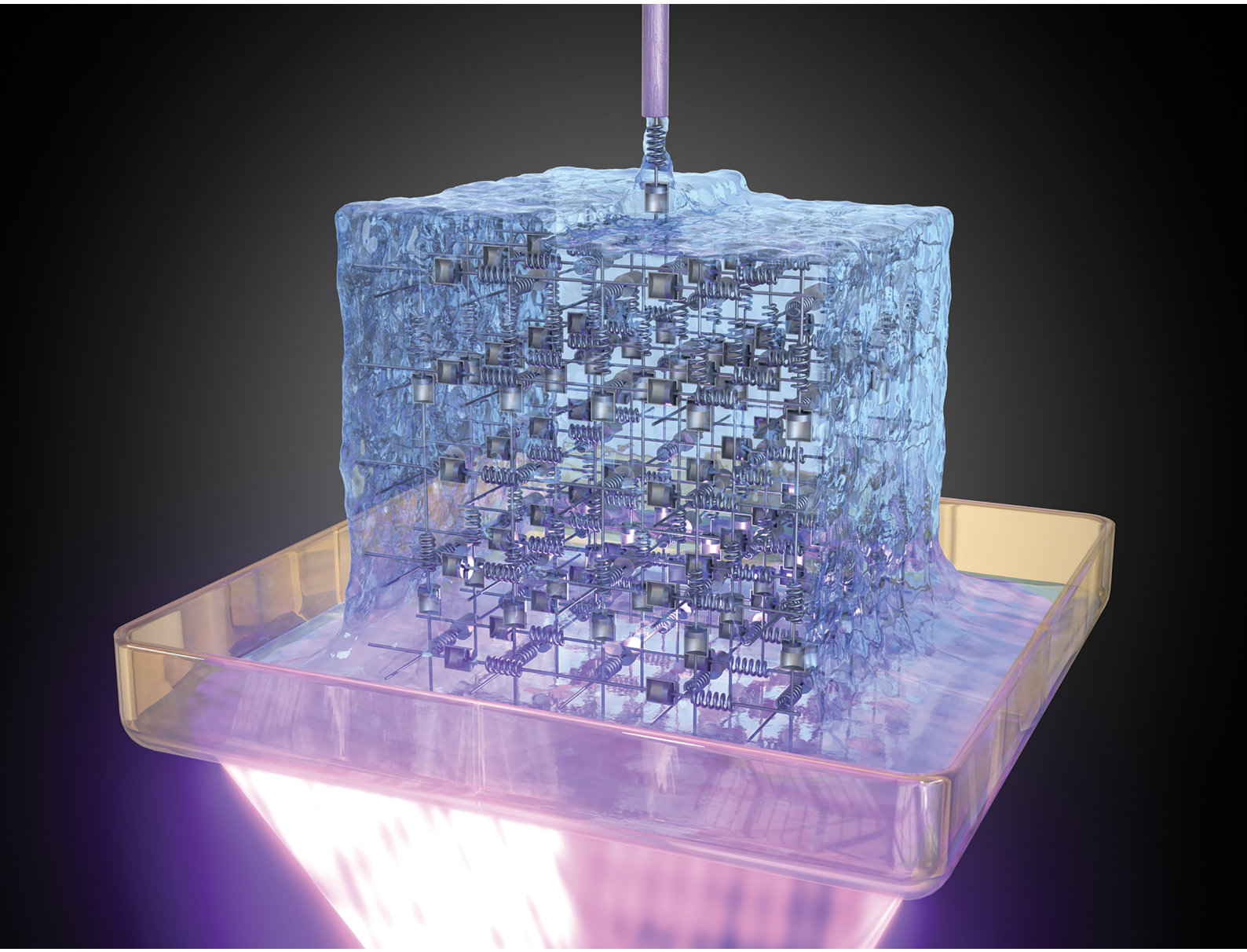

ISSN 2633-5409

ROYAL SOCIETY OF CHEMISTRY

REVIEW ARTICLE

Mercedes Fernández, Carmen Mijangos *et al.*
From rheological concepts to additive manufacturing assessment of hydrogel-based materials for advanced bioprinting applications

Materials Advances

ROYAL SOCIETY OF CHEMISTRY

REVIEW

View Article Online
View Journal | View Issue

Cite this: *Mater. Adv.*, 2025, **6**, 4566

From rheological concepts to additive manufacturing assessment of hydrogel-based materials for advanced bioprinting applications

M. Itxaso Calafel,[a] Miryam Criado-Gonzalez,[ab] Robert Aguirresarobe,[a] Mercedes Fernández*[a] and Carmen Mijangos*[bc]

Hydrogels have emerged as highly attractive polymer-based materials owing to their unique solid–liquid rheological duality, which allows their use in 3D extrusion and inkjet printing, particularly in the field of biomedical applications. The dynamic moduli (storage modulus, G', and loss modulus, G''), relaxation modulus, shear-thinning behaviour, thixotropy, viscoelasticity, and yield stress are the most commonly employed rheological concepts for hydrogel applications in 3D/4D additive manufacturing. Extrusion, inkjet printing, and stereolithography are the most studied manufacturing technologies for hydrogel bioprinting applications. Moreover, hydrogels exhibit a combination of cohesive properties of solids and the transport characteristics of liquids. Their rheological behaviour, however, varies depending on whether they are chemically cross-linked, showing a pure solid elastic behaviour, or physically crosslinked, showing viscoelastic behaviour. While rheology reveals much information about the flow behaviour of liquids or deformation behaviour of solids, it is not as obvious as to anticipate the printability of hydrogels. Therefore, a deep understanding of rheological principles and their correlation with printability is essential. This review begins summarizing various polymer hydrogels. Subsequently, the definition and description of the most employed concepts, namely relaxation modulus, storage, and loss moduli, and many others, are necessary to understand and associate the feasibility of hydrogels for a particular bioprinting process. This review mainly addresses: (i) rheological determination of the processing window for direct ink writing (DIW), (ii) rheological restrictions for printing beyond direct ink writing (DIW), and (iii) vat photopolymerization bioprinting and the biological implications of bioprinting. Finally, all the above concepts are illustrated with a few examples of biomedical applications of 3D/4D printed hydrogels.

Received 9th January 2025,
Accepted 14th May 2025

DOI: 10.1039/d5ma00019j

rsc.li/materials-advances

1. Introduction

Rheology is the scientific basis for the additive manufacturing (AM) of hydrogels or other polymer-based materials, although it has not always been taken into consideration. As known, the growth of 3D and 4D additive manufacturing techniques has led to a revolution because they offer the possibility of producing highly customised products for specific applications that can be designed and fabricated locally.[1–10] The concept of additive manufacturing encompasses different manufacturing technologies. According to the method used to form the final product (ASTM F42), they have been categorized into seven main processes: material jetting (a drop by drop of build material is selectively deposited), binder jetting (a liquid binding agent is selectively deposited to join powder particles, typically metal, sand and ceramics), vat photopolymerization (photopolymerizable resin is selectively cured by a light source), powder bed fusion (electron beam or laser is used to melt or weld the material powder), material extrusion (material is extruded through a nozzle which usually is at high temperature), energy deposition (similar to material extrusion, the nozzle is not fixed to a specific axis and can move in multiple directions), and sheet lamination (sheets of materials are bonded together and cut to shape).[11–18]

One of the most promising materials for additive manufacturing are hydrogels. While hydrogels are not traditionally associated with additive manufacturing, there have been significant developments in 3D printing hydrogels in recent years (Fig. 1), particularly in the biomedical field. Bioprintig is one of the primary applications of 3D printing hydrogels, as living

[a] *POLYMAT and Faculty of Chemistry, University of the Basque Country UPV/EHU, Paseo Manuel de Lardizabal 3, 20018 Donostia-San Sebastián, Spain. E-mail: mercedes.fernandez@ehu.eus*
[b] *Instituto de Ciencia y Tecnología de Polímeros (ICTP-CSIC), Juan de la Cierva 3, Madrid 28006, Spain. E-mail: cmijangos@ictp.csic.es*
[c] *Donostia International Physics Center (DIPC), Paseo Manuel Lardizabal 4, 20018 Donostia-San Sebastian, Spain*

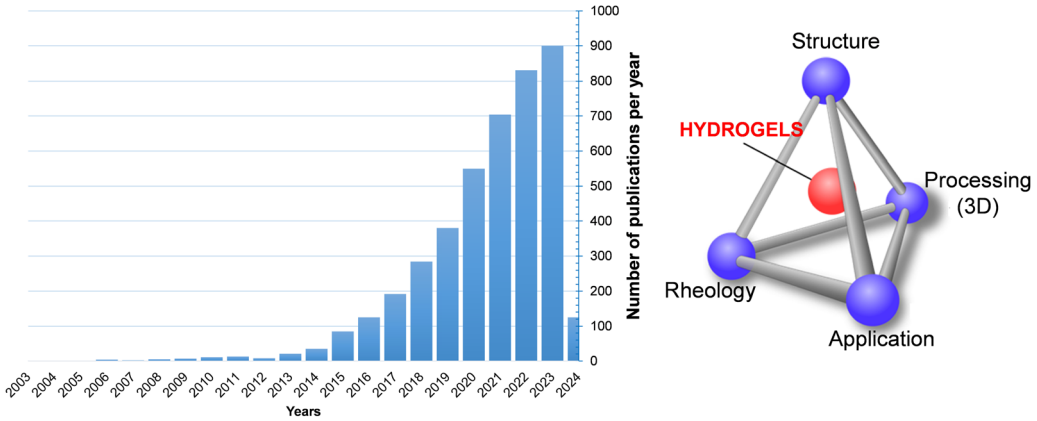

Fig. 1 Bar chart showing the growing interest in hydrogels between 2006 and 2024 (left). Schematic showing the interrelationship between the structure, rheology, processing and application of polymer hydrogels.

cells are combined with hydrogel polymeric materials to create tissue-like structures. These structures can mimic the complex architecture of natural tissues and organs, making them valuable for applications in regenerative medicine, drug testing, and disease modelling. Furthermore, 3D printing allows precise control of the geometry and internal structure of the hydrogel. This level of hierarchy or customisation enables the fabrication of complex tissue scaffolds with specific mechanical properties and biofuntionalities tailored to the intended application. The main 3D printing processes used for fabricating hydrogels include extrusion-based 3D printing (direct ink writing, DIW), vat photopolymerization (stereolithography (SLA) and digital processing (DLP)) and inject-based processes. Despite the promising potential of 3D printing hydrogels, several challenges remain, including achieving high-resolution printing, maintaining cell viability throughout the printing process, and controlling the mechanical properties of the printed constructs. Many of these challenges are related to the viscoelastic properties of the hydrogels and their ability to regenerate or recover after printing. In the case of material extrusion 3D printing process, hydrogels are forced through a nozzle that moves at a predetermined rate, being deposited on a static platform; therefore, they are subjected to shear, elongational, and compression forces or a combination of all these forces, leading to variations in their rheological properties. In contrast, vat photopolymerization depends on the flow of the polymer resin to fill the void created by platform movement during printing, along with precisely controlled light exposure—both in duration and intensity—to initiate polymerization while preventing overcuring.[19] Obviously, any of the above processes brings about changes in the hydrogel or polymer material that could compromise the final material performance, as it is reflected in the schematic interrelationship between the structure, rheology, processing and application of Fig. 1.

In order to assess the potential of a hydrogel as a 3D bioink or injectable material, it is crucial to identify the rheological properties that allow us to understand and anticipate the performance of the resulting three-dimensional (3D) structures. Pseudo plasticity, viscosity and ratio G'/G'' and quick gelation (gelation time), shear-thinning behaviour, the yield stress (critical stress), self-healing/recovery are the most important characteristic properties that would identify the injectability and self-healing ability of the hydrogel and, definitely, the feasibility of the AM. The viscosity of a hydrogel determines how easily it flows through the printer nozzle during extrusion. Hydrogels with higher viscosities may require higher printing temperatures or pressures to facilitate extrusion, whereas low-viscosity hydrogels may be prone to sagging or spreading after deposition. Regarding shear-thinning behaviour, many hydrogels show a viscosity decrease under shear stresses and, therefore, facilitate the extrusion and allow finer control over filament deposition. On the other hand, many other hydrogels also exhibit thixotropic properties (Section 2.3.4), which allows hydrogel ink to regain its initial viscosity/structure when printing pauses, thereby preventing excessive spreading or deformation of the printed layers. Gelation kinetics are intimately related to the consistency of the hydrogel itself. Rheological measurements can provide insight into the gelation kinetics of hydrogel precursors, including the onset of gelation, gelation time, and gel strength development. Controlling gelation kinetics is critical for ensuring proper layer adhesion, dimensional accuracy, and structural integrity of the printed parts. In the case of vat photopolymerization, the flow of the polymer and the spatial control of light (exposure light and time, especially) are crucial parameters of the process. The material must present adequate flow properties to fill the gap left by the movable platform during printing. Therefore, proper resin flow helps maintain a stable liquid level in the vat, preventing interruption in the printing process because of insufficient material. On the other hand, spatial control of light, typically a UV laser or a digital projector (DLP), provides selective cure for photopolymer resin in specific areas corresponding to the cross-section of the desired part. This involves the control of exposure parameters, such as light intensity, exposure time, and light wavelength, as they directly affect the polymerization rate and degree of crosslinking. Since 3D printing has aroused so much interest, some general reviews and specific works related to the rheological behaviour of a particular hydrogel

or of a particular application, has already been published.[20–27] Most reviews although very exhaustive from emerging biomedical application point of view, do not refer to rheological concepts.[8]

The most demanded application of hydrogel-based 3D printing is in the area of biomedicine and the most representative selection are tissue engineering, surgical reparation, drug delivery and bioelectronic, among others.[20–27] Beyond polymer-only hydrogels, cell-laden hydrogels are among the most widely utilized. Consequently, the cartridge temperature is usually defined in the range of 30–40 °C (allowing cell survival) and the printing pressure is 100–200 kPa (reducing cell stress). The addition of cells after hydrogel bioprinting minimises the importance of these parameters. Mesenchymal stem cell lines (MSCs) are the most commonly used cell line in combination with hydrogels. In general, good viability results were obtained for all cell lines. Regarding mechanical tests, the Young's modulus is widely used in bioprinting, although there is no consensus on the most important mechanical properties of each bioprinted structure.

It is obvious that after the manufacturing process, the final material needs to fulfil a series of requirements depending on the final application. For applications such as cartilage, bone, skin, nervous, vascular, neural stem cells, skin tissue reconstruction, and many/similar applications, flexibility, stiffness, mechanical strength, and recovery are the required polymer properties for hydrogels, in addition to biocompatibility, biodegradability, anti-inflammatory effects and antimicrobial properties. This type of studies have been part of many different research works or specific reviews. For this reason, the reviews focused on specific applications of hydrogels, such as plastic surgery or orthopaedic applications; therefore, they will not be included in the present review. As an example, see the ref. 28.

In summary, this review is addressed to briefly introduce the hydrogels, including the definition of gel structure and the correlation to rheological properties/concepts, as well as to define the fundamental rheological concepts to assess the good printability of hydrogels, in general, and not for a specific purpose. It also describes the information that can be obtained from a simple torsional rheometer or an optical rheometer. Moreover, an important part is addressed for different bioprinting technologies, and finally, some specific examples are developed from a practical perspective.

2. Hydrogels

Gels, which are three-dimensional polymeric structures, have proven to be effective storage/incorporation systems for solvents and other components as well as important vehicles for drug release and magnetic hyperthermia. Polymer hydrogels, made up of polymers and water, have both cohesive properties of solids and transport properties of liquids. This duality allows for the modulation of the activity of the gels in a controlled manner and their use as a 3D extrusion material. Gels cover a wide spectrum of polymers (synthetic and natural), sizes (macro, micro, and nanogels), and specific properties, which are very attractive for their applications.

Common polymers used for hydrogels include synthetic polymers such as polyethylene glycol (PEG), poly(vinyl alcohol) (PVA), poly(*N*-isopropylacrylamide) (pNIPAAm), poly(acrylic acid) (PAA), and poly(2-hydroxy ethyl methacrylate) (PHEMA) and other acrylics, and natural ones including collagen, hyaluronic, and bio-based polysaccharides such as alginate, gelatin, agarose, cellulose and chitosan. Nevertheless, it is not yet clear the relationship between the chemical structure (composition and formulation) of hydrogels, the good printability of hydrogels, and the final behaviour of bioprinted structures. Therefore, for a given polymer–solvent (water) system, it is not possible to predict its gel-forming capacity, nor determine the key process in the gelation phenomenon or how the structure of a gel affects its properties; even so, the forming systems of gels have found numerous specific applications in many sectors of medicine, agriculture, food, *etc.* when a 3D bioprinter is used. A systematic review on hydrogels for bioprinting has been recently reported, based on a Prisma methodology.[5] Authors conclude that (i) alginate is the most commonly used material followed by gelatin and gelatin-methacrylamide (GelMA), (ii) the most used concentrations for these three polymers are 2–4% for alginate, 5% for gelatin and 10% w/v for GelMA, respectively and (iii) the preferred cross-linking methods are chemical and based on Ca^{2+} cations for alginate; thermally induced for the physical cross-linking of gelatin and UV light as the standard cross-linking for GelMA.[5] Among other many hydrogel precursor materials, hyaluronic acid (HA) has become the one of the most attractive hydrogels precursor for bioinks due to its excellent physicochemical and biological properties, such as biocompatibility, hydrophilicity, non-immunogenicity, and complete biodegradability.[28] Recently, the gel-like cellulose nanofibrils (CNFs) have attracted increasing attention as an ingredient when formulating the bio(material) inks for hydrogel extrusion-based 3D bioprinting attributed to structural similarity to extracellular matrix, low cytotoxicity, and desirable rheological properties.[4] The importance of elastin and its role in auricular cartilage tissue engineering has also been deeply studied.[29] Elastin is a highly insoluble structural protein that is rich in hydrophobic amino acids, scarce in polar groups, and found in the extracellular matrix (ECM) of elastic tissues. Elastin plays essential mechanical and biological roles in its occurrence, including the flexibility of the tissue and interactions with cells through specific biochemical and biophysical processes.

Hydrogels can be broadly categorised into physical and chemical hydrogels based on the interactions that join their network structures (Fig. 2). Physical hydrogels are mainly formed through physical interactions such as hydrogen bonding, hydrophobic interactions, electrostatic interactions or physical entanglements of polymer chains (Fig. 2a). The physical interactions between different polymer chains prevent the hydrogel from dissolving, thereby maintaining the structural integrity. Nevertheless, these hydrogels often acquire poor mechanical properties due to the weak nature of this type of crosslinking.

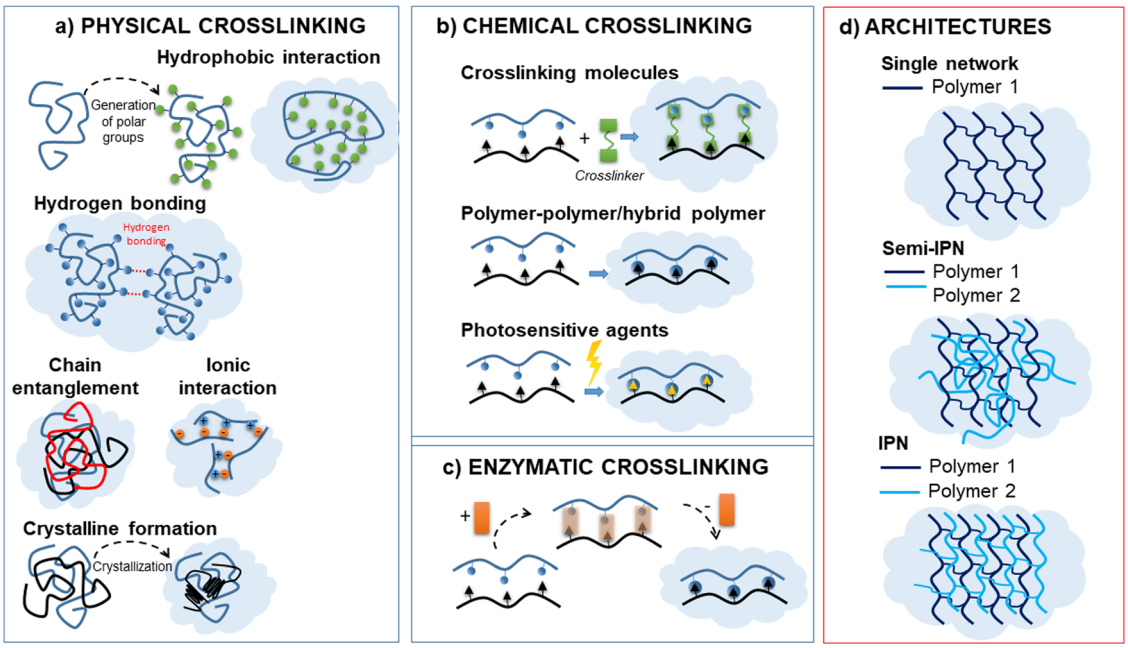

Fig. 2 Schematic representation of the different routes of formation of a polymer hydrogel: physical crosslinking (a), chemical crosslinking (b), enzymatic crosslinking (c) and its potential macromolecular structures (d).

These interactions are reversible and can be disrupted by changes in environmental conditions such as temperature, pH, or ionic strength. Physical hydrogels typically exhibit properties such as shear-thinning behaviour (reduced viscosity under shear stress) and self-healing. Examples of physical hydrogels include those based on polymers, such us polyethylene glycol (PEG) or natural polymers like gelatin or alginate. However, chemical hydrogels are formed through the covalent crosslinking of polymer chains, leading to stable covalent bonds within the hydrogel network (Fig. 2b and c). Polymer chains can be joined through use of crosslinking molecules or can be directly bound to each other. It mainly involves Schiff base reaction, Michael addition reaction, free radical polymerization, click chemistry, and enzyme crosslinking.[30,31] Chemical hydrogels have stable network structures and are irreversible under normal conditions. They often exhibit tuneable mechanical properties and degradation rates based on the choice of the crosslinking chemistry. Examples of chemical hydrogels include those based on synthetic polymers, such us polyacrylamide or polyvinyl alcohol, as well as natural polymers like hyaluronic acid or collagen. Polyacrylamide hydrogels are typically cross-linked with agents such as *N*,*N*′-methylenebisacrylamide (MBAA), and poly(vinyl alcohol)-based hydrogels are cross-linked with glutaraldehyde. However, polyethylene glycol-based hydrogels can be created through the covalent cross-linking of PEG chains, utilizing either photopolymerization or chemical agents. On the other hand, alginate hydrogels, which are primarily modified with functional groups, form chemically cross-linked hydrogels *via* UV curing. To obtain versatile biomaterials with enhanced performance, advanced architectures have been developed (Fig. 2d).[32] Hydrogels can be comprised of either a single component forming a physical or chemical network or multiple polymer components. Particularly, when two polymers are cross-linked, but not covalently bonding to each other, the resulting materials are known as "interpenetrating polymer networks" (IPN). In these networks, the polymers are physically entangled and cannot be separated unless chemical bonds are broken. This type of hydrogel typically exhibits enhanced mechanical strength, stability, and swelling behaviour; a common example is the system of polyacrylamide (PAAm) and alginate.[33] Conversely, if one or more linear (non-cross-linked) polymer are entangled with the cross-linked one, the resulting structure is referred to as a "semi-interpenetrating polymer network" (semi-IPN). These semi-IPN systems are particularly useful for controlled drug release due to tuneable porosity.[34] Finally, hybrid gels were designed to obtain stimuli-responsive polymer systems. The incorporation of inorganic nanoparticles, such as gold or magnetic nanoparticles, provides additional functionalities such as light or magnetic responsiveness, respectively.

Concerning the size of hydrogels, macro- and microgels are the most used in AM. There are several definitions for macrogels. (i) Macrogels tend to adopt the shape of the container or (ii) a macrogel immersed in excess solvent must be swollen but not solved (or dispersed), whereas microgels are colloidal particles dispersed in a solvent. The formation of a chemical macrogel (tridimensional network) depends on the crosslinker, polymer concentration, temperature, solvent, and time (aging has been observed in many polymers). The formation of a physical macrogel depends on the chemical or physical nature of crosslinking points of the network (crystal origin, interactions, *etc.*). Microgel dispersions combine the properties of hydrogels with the particularities of colloidal systems, and depending on their composition, they can quickly respond (much quicker than a macrogel) to external stimuli.[35] In most

applications, microgels are subjected to shear, elongation, and compression, or their self-assembly is required. Therefore, their behaviour under such conditions has a direct effect on the final material performance.

A priori, it is difficult to define which specific gel is more appropriate for a particular 3D processing technology and a specific application. In recent years, the concept of 4D printing has also been considered. 4D bioprinting is an advanced form of 3D bioprinting that adds the dimension of time to the process. It involves printing biological structures that can change shape, function, or behaviour over time in response to external stimuli such as temperature, humidity, pH, light, or magnetic fields.[25] In this context, although a direct relationship between the structure of the gel and its bioprintability has not been established, semi-interpenetrated gels seem more suitable candidates (see Section 4). Nevertheless, studying the viscoelastic properties of a particular hydrogel, as a function of preparation conditions, would allow anticipating its viability for bioprinting.

Depending on the type of gel, chemical or physical and macro or micro gels, different theories relates the density of network chains to the elastic modulus and therefore to 3D applications. The dependence of the modulus on concentration for chemical and thermoreversible macrogels and microgels is widely reported in the literature.[36] For instance, in the case of chemical macrogels, the theory of rubber elasticity, proposed by James and Guth and later expanded by Treloar and Kuhn,[37,38] predicts a relationship between elastic modulus and concentration of gel, defined by the following equation (eqn (1)):

$$G = NkT = \frac{\rho RT}{M_c} \quad (1)$$

where N is the number of chains/volume, K is the Boltzmann constant, T is temperature, R is the gas constant, ρ is the density of the network, and M_c is the molecular weight between entanglements.

Although physical, chemical and interpenetrated gels are used for AM, their rheological behaviour is very different between them. For instance, physical gels are relatively easily deformable and can be disrupted by temperature or environmental changes, whereas interpenetrated gels can add plasticity to the system. The rheological properties depend not only on the nature of the ''crosslinking'' (in this case also understanding as ''crosslinking'' points physical entanglements) but on the chemical nature of polymers and the polymer concentration, so, it is very difficult to associate or to anticipate hydrogel performance based uniquely on its structure and, therefore, the use of a specific gel for a particular application. Until the present, it has not been reported such a general correlation, but some particular studies have been carried out, for instance, that in which the printability of a double network alginate-based hydrogel for 3D bio-printed complex structures has been analyzed.[26] Unlike linear polymers, microgels show an increase in viscosity through a different mechanism. At low concentrations, both linear polymers and microgels show an increase in viscosity proportional to the product of intrinsic viscosity and concentration. However, at high concentrations, linear polymers become entangled, resulting in a rapid increase in viscosity, while microgels become packed and confined by their neighbours – colloidal arrest – leading to a further increase in viscosity, faster than in linear polymers.[35,39] Furthermore, from a certain concentration and at low stresses, the microgel dispersions present a behaviour similar to that of a solid. Particularly attractive are the viscoelastic/viscoplastic gels. When a viscoelastic/viscoplastic gel is submitted to an applied force, the polymer network can reorganize itself or have dissipative mechanisms, by disrupting or rearranging the crosslinks in the network. To achieve this, several strategies have been employed, such as the use of ionic crosslinking, host–guest or other supramolecular interactions or the introduction of dynamic covalent bonds and hydrophobic interactions. In the case of 3D bioprinting of microgels or nanogels, they are subjected to shearing, deformation, or compression conditions and, therefore, it is crucial to determine and interpret the rheological properties of microgel dispersions. Furthermore, rheology is presented as a tool to explore the existence of interactions between microgels, interactions that can lead to the formation of more complex structures that can be predicted with the aid of fractal theories and even determine the minimum critical solution temperature.[40]

3. Rheological concepts and tools

Rheology offers crucial insights into both the flow of liquids and the deformation of solids, making it a fundamental tool in understanding the behaviour of polymeric gels used in biofabrication. In hydrogel-based 3D printing, rheological properties influence two critical aspects: (1) the printability of the bioink, and (2) the mechanical performance and stability of the resulting printed construct. These two aspects require the understanding of different rheological properties. Rheology devoted to structural characterization elucidates the material's intrinsic viscoelastic response under small, well-controlled deformations, offering insights into crosslinking density, relaxation mechanisms, and other microstructural features. In contrast, processing rheology addresses how bioinks behave under the non-linear, often large deformations and high shear rates encountered during manufacturing processes such as extrusion or jetting.

In hydrogels, complex rheological behaviour is intrinsically linked to their molecular architecture. Hydrogels formed *via* covalent crosslinking exhibit predominantly elastic responses, with stress stored rather than dissipated. Conversely, physically crosslinked (reversible) hydrogels exhibit viscoelastic behaviour and non-Newtonian flow due to the dynamic nature of their intermolecular interactions.[41] This complexity is advantageous across applications in pharmaceuticals, biomedicine, energy, environmental science, and food technology, where tailored rheological profiles are essential.[42]

Consequently, hydrogels for additive manufacturing display multifaceted rheology that cannot be captured by a single property such as zero-shear viscosity (η_0) or elastic modulus

(G'). Instead, full characterization must include the viscoelastic properties storage (elastic) and loss (viscous) modulus and the transient responses of creep/recovery and relaxation modulus, as well as shear rate – dependent viscosity, yield stress and thixotropy. Those are different aspects of viscoelastic and viscoplastic behaviour that characterize hydrogels. Viscoelasticity, which depends on the time scale of deformation, combines both solid-like (elastic) and liquid-like (viscous) responses.[2] Importantly, viscoelasticity is a key design property for biomaterials in regenerative medicine, as biological tissues are inherently time-dependent materials that dissipate energy during deformation rather than behaving as ideal elastic solids.[43] Viscoplasticity, or yield stress behaviour, adds another dimension by allowing hydrogels to act as solids below a critical stress threshold, providing *in situ* structural support, while flowing as liquids once that threshold is exceeded. This is especially important for preventing nozzle clogging and feature collapse during extrusion printing.[44] Furthermore, non-linear viscous behaviours such as shear thinning (pseudoplasticity) and thixotropy govern both the extrusion process and the recovery of structure post-deposition, enhancing print smoothness, layer adhesion, and shape retention.[45] Thixotropy refers to the time dependency of viscosity induced by flow. Such behaviour has been reported for printing inks, and it can be easily confused with viscoelastic responses.[46,47] In injectable hydrogels, these properties also facilitate spatiotemporal control over drug release.[48]

The primary flow types relevant to 3D printing are shear and elongational flows. In extrusion-based printing, simple shear flow dominates within the nozzle, while elongation flows occur at localized regions like nozzle entrances and during deposition. While shear flows are relatively easy to generate and control across a broad range of shear rates and stresses, elongation flows are harder to replicate experimentally. Therefore, our focus is mainly on the rheological characterization of hydrogels with attention to shear rheometry. For further information on the importance of extensional rheological behaviour and its influence on 3D printing processing, we refer to well-comprehensive review articles.[49–51]

Torsional and capillary rheometers are the most commonly employed tools for evaluating shear rheology.[2] Torsional rheometers apply oscillatory or continuous shear between two surfaces, one stationary, whereas capillary rheometers can access higher shear rates (100–10 000 s^{-1}), approximating those during direct ink writing (DIW). These residence times are on the order of milliseconds, much longer than in inkjet printing, where they are closer to 10 μs.[52] Oscillatory shear rheology, in particular, allows modulation of amplitude and frequency, thus probing material behaviour across various timescales. It also differentiates between linear viscoelasticity at small deformations—where structure remains largely intact,[40,53–55] and non-linear behaviour at large deformations, where network stretching,[2,40,56,57] yielding, or even structural breakdown can occur. Such studies are essential to evaluating printability under conditions that closely mimic actual processing. Table 1 summarizes the important rheological properties for the three most widely used hydrogel-printing techniques: material extrusion, material jetting, and vat photopolymerization.

The subsequent sections will explore these critical rheological properties, highlighting their roles in both processability and the interplay between rheology, network structure, and end-use applications of printed constructs.

3.1. Linear viscoelasticity. Rheological properties: $G(t)$, $J(t)$, $G'(\omega)$ and $G''(\omega)$

Viscoelasticity is the property of materials that exhibit both viscous and elastic characteristics when deformed. Elastic deformation is instantaneous, as opposed to viscous deformation in which there is always a time delay between the application of the external load force and its subsequent deformation. Moreover, unlike elasticity, viscous deformations cannot be recovered or reversed when the external force is released. Therefore, the properties of viscoelastic materials are those for which the stress–strain relationship depends on time, involving storage and loss of energy, fluid memory, and time dependence. These relationships are described by the main viscoelastic functions: (1) the relaxation modulus, $G(t)$, that

Table 1 Rheological properties of hydrogels for 3D printing

Rheological properties influencing printing process			
Printing method	Key rheological properties	Typical or critical values for hydrogels	Ref.
Extrusion-based (DIW)	Viscosity (η) Yield stress (σ_y) Shear-thinning index (n) Storage modulus (G') Recovery time/self-healing	• η: 10^2–10^6 mPa s (at approx. 0.1 s^{-1}) • τ_y: 10–1000 Pa (enables shape fidelity) • $n \approx$ 0.3–0.6 (pronounced shear-thinning for smooth extrusion) • G': 100–10^4 Pa (must be $G' > G''$ for structural integrity and fidelity) • Post-printing recovery: <10 s after cessation of shear for high fidelity preservation of shapes	2, 53 and 57–61
Inkjet printing	Low shear viscosity Storage modulus, G' Surface tension	• $\eta <$ 10–20 mPa s (for droplet ejection) • Low elasticity to prevent clogging/satellite drops • Surface tension: 30–50 mN m^{-1}	61–64
Vat photopolymerization with hydrogel precursors	Low-shear viscosity Photocuring rate: G' evolution during/after curing Light penetration depth	• $\eta <$ 5 Pa s (to ensure smooth recoating) • Gelation: within ~seconds: G' increases rapidly post-exposure with final G' often $>10^3$ Pa • Critical for resolution (~100–1000 μm depth range)	65

quantifies time-dependent relaxation after imposed a deformation, (2) the time-dependent creep compliance, $J(t)$, and (3) oscillatory stress–strain phase shift that can reveal decomposed storage and loss moduli, G' and G'', respectively. All of these functions are interrelated in the limit of linear viscoelasticity (LVE) at small strain or stresses.[66] Therefore, the linear viscoelastic properties, including the dynamic moduli ($G'(\omega)$ and $G''(\omega)$), relaxation modulus and compliance ($G(t)$ and $J(t)$), are unique features of the material structure, because they do not depend on the applied strain or strain rate and will inform us about the equilibrium structure of the hydrogels, offering insight into the viscoelastic memory and long-term behaviour of hydrogels. These parameters are directly influenced by the molecular arrangement and interactions within the material.

Typically, measurements are made at the macroscopic scale using dynamic mechanical analysers or rheometers, based on experiments and equations that allow us to experimentally access these functions and which are described in detail below. It should also be noted that alternatively, measurements can be made at the microscopic scale using microrheology and scattering.

3.1.1. The relaxation modulus $G(t)$. In a first approach, the stress relaxation test gives valuable information about the feasibility of a hydrogel for 3D additive manufacturing. During the test, a constant deformation, γ_0, is applied, and the resulting stress is recorded as a function of time. The relaxation modulus, $G(t)$, that measures the resistance to deformation, is recorded as the proportionality between the time-dependent stress, $\sigma(t)$ and the imposed deformation, γ_0:

$$G(t) = \frac{\sigma(t)}{\gamma_0} \tag{2}$$

$G(t)$ provides information about hydrogel's network dynamics [Fig. 3]. An elastic, covalently cross-linked hydrogel, would keep the stress almost constant during the experiment, while soft hydrogels, in which dynamic fluctuations and rearrangements occur within the microstructure, would behave like a viscoelastic material and would relax some of the stress over time [Fig. 3a].

Modelling the stress relaxation behaviour is key to further investigating the viscoelastic response of hydrogels. Considering linear viscoelastic conditions, (LVE), the stress relaxation response can be understood from the exact solutions to the step deformations by applying Maxwell's model. The Maxwell model establishes the relationships between deformation and stresses using a mechanical combination of a Hookean spring and dashpot in series which give rise to a viscoelastic stress relaxation governed by a single time-scale, τ:

$$G(t) = \frac{\sigma(t)}{\gamma_0} = G\exp\left(-\frac{t}{\tau}\right) \tag{3}$$

where $G = \frac{\sigma_0}{\gamma_0}$ and $\tau = \frac{\eta}{G}$, the ratio of the dashpot viscosity, η, to the spring modulus, G, defines the relaxation time of the Maxwell model. This represents the time required for the stress to decay from its initial value, σ_0, to $\frac{\sigma_0}{e}$ (*i.e.* approximately $0.37\sigma_0$).

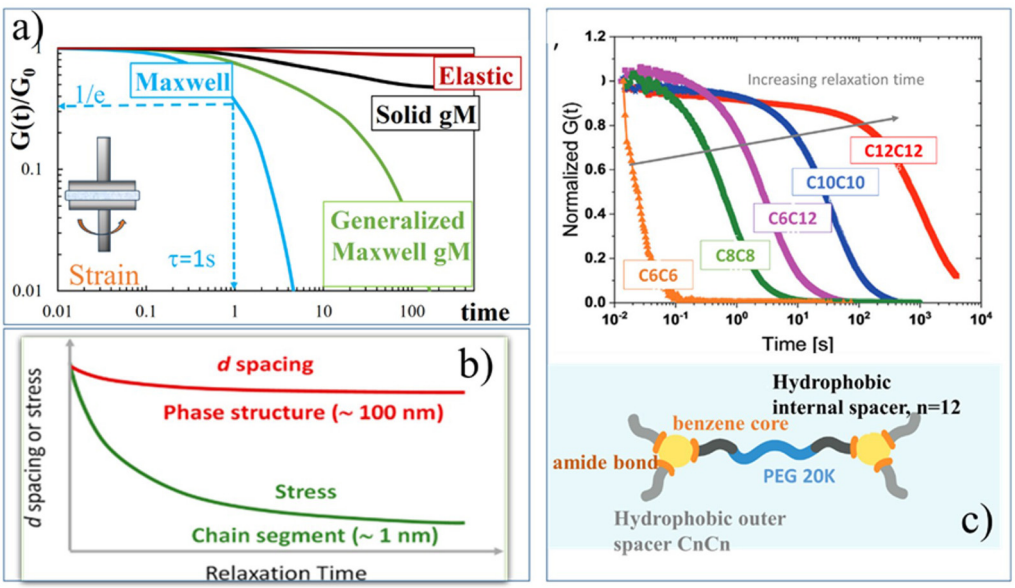

Fig. 3 Linear viscoelastic properties. Relaxation modulus, $G(t)$: (a) Maxwell-based models for the stress relaxation behaviour. The elastic response with nearly constant stress over time, and the viscoelastic response with time-dependent stress relaxation modelled using Maxwell-based equations: the classical Maxwell model (eqn (3)), the generalized Maxwell model (gM) (eqn (4)), and the solid generalized Maxwell model (solid gM) (eqn (5)), (b) stress relaxation behaviour revealing multiscale architecture in polyampholyte hydrogels. Rapid stress relaxation arises from chain segmental rearrangement (~1 nm) *via* reversible ionic bond breakage, while slower relaxation corresponds to reorganization of structural domains (~100 nm). Adapted with permission from ref. 67 Copyright © 2020, American Chemical Society, (c) broad spectrum of relaxation times (0.1–10^3 s) observed in benzene-1,3,5-tricarboxamide (BTA) supramolecular fibrous hydrogels. Increasing the hydrophobic outer spacer length (CnCn) leads to reduced viscoelasticity and longer average stress-relaxation times, reflecting changes in dynamic network stability. Adapted from ref. 68. Copyright © 2023, Wiley.

As illustrated in Fig. 3a, the stress relaxation curve predicted by the classical Maxwell model shows a strong decrease from 1 to near zero, at $t = \tau$, indicative of a viscoelastic liquid-like behaviour. However, this decay is typically less abrupt due to the presence of multiple relaxation mechanisms. In such cases, the generalized Maxwell model, gM (also referred as the Maxwell–Weichert model, eqn (4)), which consists of several Maxwell elements arranged in parallel, provides a more accurate description of the material's viscoelastic response.

$$G(t) = \sum_{i=1}^{N} G_i \exp\left(-\frac{t}{\tau_i}\right) \quad (4)$$

Alternatively, viscoelastic solid-like behaviour can be described using the standard linear solid model, which consists of a Maxwell element (a spring and a dashpot in series) arranged in parallel with an additional spring, $G(t) = \frac{\sigma(t)}{\gamma_0} = G_e + G\exp\left(-\frac{t}{\tau}\right)$, or to the generalized linear solid model (solid gM) in eqn (5):

$$G(t) = G_e + \sum_{i=1}^{N} G_i \exp\left(-\frac{t}{\tau_i}\right) \quad (5)$$

where G_e represents the long-term equilibrium or rubber elastic modulus of the hydrogel network.

Although most viscoelastic stress relaxation responses of hydrogels deviate from single exponential decay, exceptional cases exhibiting essentially Maxwellian behaviour have been described. A prototypical example includes transient polymeric networks, such as reversibly crosslinked hydrogels formed *via* dynamic chemistry.[69,70] These materials are particularly attractive due to their shear-sensitive nature, which leads to shear-thinning behaviour, desirable for printable and injectable hydrogel formulations. Nevertheless, in the majority of hydrogels systems, the viscoelastic response is significantly more complex than predicted by classical the Maxwell model of linear viscoelasticity. This complexity arises from a broad distribution of relaxation times, typically attributed to the presence of multiple structural length scales and dynamic interactions within the network. Modelling such behaviour is non-trivial. A comprehensive review by Song *et al.*[71] provides advanced insight into this topic, offering mechanical analogue models and theoretical frameworks that go beyond the Maxwell paradigm. These tools enable a more accurate description of non-Maxwellian relaxation behaviour and facilitate a deeper understanding of the molecular and supramolecular physics governing the relaxation dynamics in increasingly diverse hydrogel families.

Stress relaxation in hydrogels arises from underlying structural reorganization phenomena, offering critical insight into both the material's dynamic behaviour and its mechanical properties with direct implications for processability in 3D printing. A compelling example is provided by Cui *et al.*[67] who investigated polyampholyte hydrogels with complex structures. As illustrated in Fig. 3b, the stress relaxation behaviour reveals a multiscale architecture, where structural features at different length scales exhibit distinct relaxation dynamics, leading to a combination of mechanical responses. Specifically, Fig. 3b schematically distinguishes between two characteristic relaxation modes: the fast and strong stress relaxation attributed to chain segment reorientation *via* the rupture of ionic bonds (on the order of $\sim$1 nm), and a slower, weaker relaxation associated with the reorganization of structural domains ($\sim$100 nm). This ability of the network to redistribute internal stresses at multiple scales has been directly correlated with macroscopic mechanical properties, particularly the self-healing capacity of the hydrogel.[69]

Furthermore, and in anticipation of the discussion in Section 5, it is noteworthy that stress relaxation capacity of hydrogels represents a critical parameter in injectable viscoelastic systems, especially in applications where 3D cell migration and proliferation must be preserved. Numerous studies have shown that hydrogel bioinks can be molecularly engineered to fine-tune viscoelasticity and shear-thinning behaviour, thereby enhancing their processability and biological functionality. For instance, Fig. 3c illustrates the behaviour of benzene-1,3,5-tricarboxamide (BTA) supramolecular fibrous hydrogels, which serve as printable, ECM-mimicking bioinks, as reported by Hafeez *et al.*[68] In this study, the viscoelastic and stress relaxation properties of the hydrogels were precisely controlled by modifying the length of the hydrophobic outer space (CnCn). Increasing the hydrophobic chain length led to longer stress relaxation times, indicating more stable and slowly relaxing network structures. In contrast, short hydrophobic chains, display rapid stress-relaxation times and form round droplets that fail to retain their fibrous architecture after injection. It was found that hydrophobic lengths exceeding 10 carbons preserved the fibrous morphology and enabled the successful fabrication of 3D structures. These findings underscore the importance of the dynamicity of the hydrogels, which governs the shear-thinning behaviour and the injectability of these materials, important properties for their application as bioinks.

3.1.2. The creep compliance $J(t)$. As a complement to stress relaxation, creep tests also provide valuable information about the architecture of hydrogels and their response during 3D additive manufacturing. In a creep experiment, a constant stress, σ_0, is applied and the resulting time-dependent strain, $\gamma(t)$ is measured. Subsequent relaxation of the material once the load is removed can also be recorded, and corresponds to the creep recovery part of the experiment. The creep compliance, $J(t)$, is defined as the proportionality between the time-dependent strain, $\gamma(t)$, and the imposed stress, σ_0:

$$J(t) = \frac{\gamma(t)}{\sigma_0} \quad (6)$$

For a viscoelastic fluid, the long-time creep increases linearly with time with a slope equal to $\frac{\sigma_0}{\eta}$, whereas for a rubber-like material, the creep increases to a constant value $\sigma_0 J_e$, where J_e is

the rubber compliance, equal to $\frac{1}{G_e}$. Since the functions $G(t)$ and $J(t)$ are interconvertible through the Boltzmann superposition theorem,[72,73] details on the application of the models for the evaluation of the creep behaviour will not be given here.

The schematic description and potential of the creep property are illustrated in Fig. 4. During additive manufacturing, a hydrogel must deform easily when an external load is applied and recover its integrity once the load is removed. Strain creep-recovery tests are particularly informative of this behaviour, as they quantify both the viscoelastic and viscoplastic components of deformation *via* the recovered and unrecovered strains, respectively (Fig. 4a). Creep compliance $J(t)$ measures the time-dependent deformation of a material under a constant stress and delineates three distinct response regimes: (i) the elastic response (discontinuous red line) as the material deforms instantaneously when stress is applied and maintains deformation without further time dependence. Defines ideal elastic solids (*e.g.*, stiff hydrogels), (ii) the viscoelastic response (continuous green line), as the material deforms gradually under constant stress and may partially (liquid viscoelastic) or fully (solid viscoelastic) recover when stress is removed. Typical printable hydrogels below yield stress are viscoelastic solids with fully recover the strain once stress is removed, and (iii) the viscoplastic response (discontinuous blue line) as the initial viscoelastic strain is followed by continuous, irreversible flow under sustained stress. This behaviour is typical when hydrogels exceed their yield stress. By analysing the shape and plateau of the $J(t)$ curve, the hydrogel's ability to flow, support, and recover throughout the printing process can be predicted, guiding the design of formulations that balance extrudability with post-printing stability.

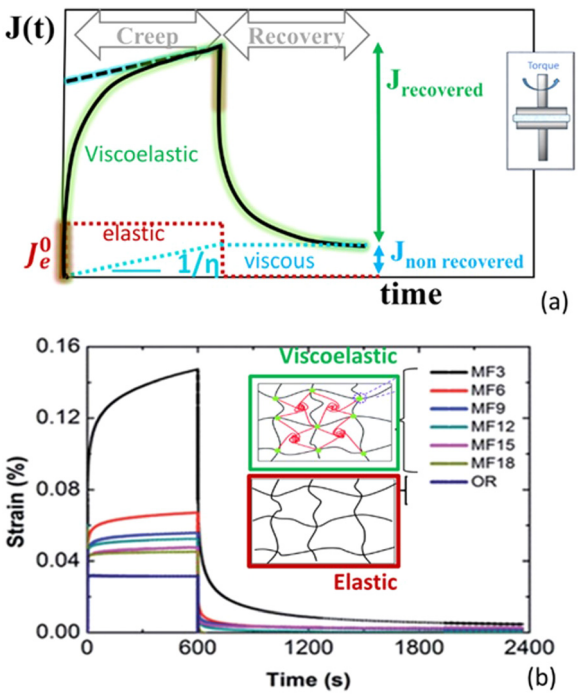

Fig. 4 Creep compliance $J(t)$: (a) creep compliance curves define elastic response (discontinuous red line), viscoelasticity (continuous green line) and viscoplasticity (discontinuous blue line); (b) creep–recovery curves comparing elastic behaviour for a purely covalently crosslinked hydrogel (OR hydrogel) with hybrid hydrogel networks bearing both covalent and reversible physical cross-links (MF series). The OR hydrogel displays negligible creep, whereas the MF hydrogels exhibit time-dependent viscoelasticity attributable to dynamic physical cross-links dissipating energy under load by stretching and disentangle processes. Data reprinted from ref. 74. Copyright © 2017 RSC.

Although some hydrogels have long been recognized to exhibit plastic behaviour, few studies have systematically quantified their permanent (unrecovered) deformation. In a recent study, Nam *et al.*[75] showed that when the applied stress exceed a certain threshold-defined as yield stress- all tested hydrogels undergo irreversible creep deformation (*i.e.*, unrecovered or plastic deformation). The concept of yield stress and its critical role in hydrogel printability and mechanical performance are discussed in detail in the dedicated "Yield stress" section.

Creep tests are also invaluable for characterizing the rheological behaviour of complex hydrogel architectures engineered to deliver a balanced viscoelastic response. Fig. 4b illustrates creep-recovery data for two series of hybrid hydrogels: one containing only covalent cross-links (denoted "OR") and another combining covalent and reversible physical cross-links (the "MF" series). In these hybrid networks, the physical cross-links form an interpenetrating polymer network that contributes to time-dependent energy dissipation—evidenced by the gradual creep and partial recovery—while the permanent covalent bonds impart instantaneous elastic response and structural integrity. This dual cross-linking strategy yields materials that both flow under load and reliably recover their form once the stress is removed.[74]

In addition, creep and creep-recovery tests are particularly useful for studying very low shear rates over long test times or under current conditions of use. This type of test would be a natural choice for measuring the viscoelastic properties of hydrogels when using stress-controlled rheometers.[71]

3.1.3. The dynamic moduli: storage $G'(\omega)$ and loss modulus $G''(\omega)$. The main rheological technique to determine the viscoelastic properties of hydrogels is the oscillatory shear test, which allows characterization of the rheological behaviour by studying the time and strain dependence separately, offering different experimental approaches that are widely used as printability criteria.[41,60,61]

The oscillatory test involves the application of a sinusoidal strain to the material: $\gamma(t) = \gamma_0 \sin(\omega t)$, measuring the stress, $\sigma(t)$, that responds to it. For a linear viscoelastic material, the stress response, in the steady state, is also sinusoidal, but is out of phase with the strain:

$$\sigma(\omega,t) = \sigma_0(\omega t + \delta) = \gamma_0[G' \sin(\omega t) + G'' \cos(\omega t)] \quad (7)$$

where δ is the phase angle or phase shift. By comparing the amplitude and δ, the storage or elastic modulus, $G' = \frac{\sigma_0}{\gamma_0}\cos\delta$, and the loss or viscous modulus $G'' = \frac{\sigma_0}{\gamma_0}\sin\delta$, can be determined as a function of frequency.

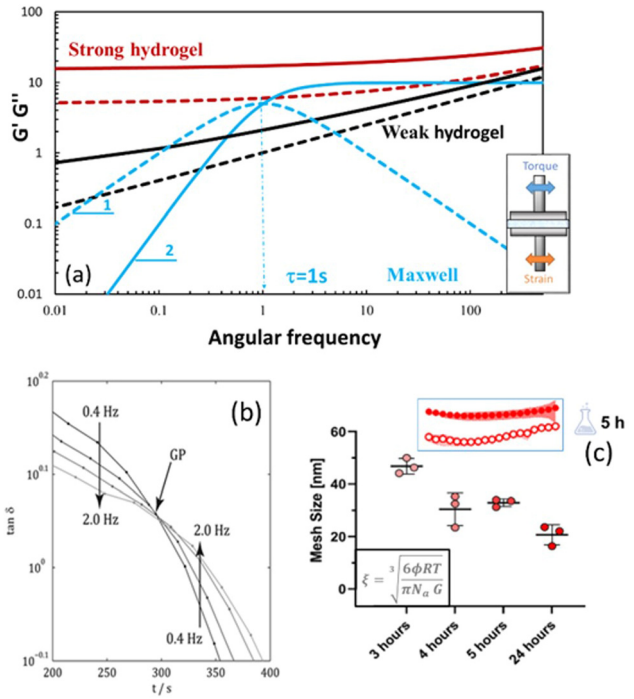

Fig. 5 Dynamic moduli: (a) Maxwell model [eqn (8) and (9)] describes the viscoelastic liquid-like behaviour; (b) gelation time from Winter and Chambon model, applied to collagen hydrogels. Data reprinted with permission from ref. 76 Copyright©2018 RSC; (c) evolution of crosslinking density (mesh size, ξ) during gelation.

The simplest liquid viscoelastic response, as already discussed, is well described by the Maxwell model with a single relaxation time. The equations describing Maxwell's model from the dynamical moduli are as follows:

$$G'(\omega) = G\frac{\omega^2\tau^2}{1+\omega^2\tau^2} \quad (8)$$

$$G''(\omega) = G\frac{\omega\tau}{1+\omega^2\tau^2} \quad (9)$$

The elastic modulus dominates at high frequencies, while the viscous modulus dominates at low frequencies, as shown in Fig. 5a. Both curves, $G'(\omega)$ and $G''(\omega)$ cross at $\omega\tau = 1$ (relaxation time, $\tau = 1$ s).

However, most of the viscoelastic responses of hydrogels need to be modelled using more than one relaxation time, and are better described by the solid generalized Maxwell model, using the following equations:

$$G'(\omega) = G_e + \sum_i Gi\frac{\omega^2\tau_i^2}{1+\omega^2\tau_i^2} \quad (10)$$

$$G''(\omega) = \sum_i Gi\frac{\omega\tau_i}{1+\omega^2\tau_i^2} \quad (11)$$

The gM solid model captures well the hydrogel behaviour. The percolated network originated from covalent crosslinking, electrostatic interactions, hydrogen bonds, hydrophobic interactions, phase separation, *etc.*, will exhibit a dominant elastic contribution, G_e, even at the lowest frequencies. In addition, various events can take place at the molecular level, including the movement of water molecules within the porous network of the hydrogel which involves additional modes of relaxation. Therefore, the discrete spectrum of relaxation times obtained from the solid generalized Maxwell model (G_e, Gi, τ_i) will provide information on the different time scales as a function of the polymer length and structure, the water strength bond and the degree of physical or chemical crosslinking. The behaviour will distinguish between true gels, for which $G'(\omega)$ and $G''(\omega)$ reach a plateau at low frequencies and weak gels for which both moduli decrease with decreasing frequencies, as seen in Fig. 5a. Strong gels do not exhibit relaxations at long time scales and form true irreversible elastic network structures over the entire frequency range, whereas weak gels, dissipate energy due to networks imperfections.[41]

Additionally, in the context of 3D printing, or injectable applications, $G''(\omega)$ is used to describe the viscous flow (representing the phenomenon of ink passing through a nozzle) and $G'(\omega)$ is related to the elastic component that influences the printing accuracy and determines the shape fidelity (after printing).[50] A proper balance between viscous and elastic modulus is required to ensure high printing accuracy and shape fidelity, as highlighted by Townsend *et al.*[77]

The oscillatory experiments to determine the structural features of hydrogels should be performed in the linear viscoelastic region (LVR), previously delimited to confirm the stability of the network in a shear environment. That is, in the linear region, the small applied deformation would not alter the microstructure of the hydrogels, so the effect of frequency on the dynamic moduli provides information on the intrinsic time scales of the hydrogel. Short time scales correspond to the local mobility or dynamics at high frequencies, while long time scales correspond to the relaxations of the long-range structures studied at low frequencies. The effects on the structure due to solvent evaporation, curing, gelation, degradation or directly the recovery of a given load application (self-healing property) can be controlled by time or temperature sweep experiments at constant frequency.

Especially relevant is the characterization of the gelation process. Time or temperature sweeps under constant frequency allow monitoring the change in viscoelastic properties that occurs during the gelation process.[78,79] A predominantly viscous pre-hydrogel state ($G' < G''$), consisting of non-interacting segments such as dangling ends, stray chains and loops, is followed by a gelation state when more networks are formed and, consequently, G' rapidly exceeds G'' ($t > t_{gel}$ or $T > T_{gel}$). For a well-developed network a solid-like behaviour is reached ($G' > G''$) and the values of the hydrogel moduli can be evaluated at equilibrium. Therefore, the time or temperature at the crossover point, $G' = G''$, although it can be considered a measure of the gelling point, is somewhat imprecise, since it depends on the frequency at which the test is performed. To avoid this uncertainty, the classical Winter and Chanbom model is commonly used, and validated for a variety of hydrogels including carboximethilcellulose,[80] gelatin,[81] collagen,[76]

and photocrosslinked alginate hydrogels[82] among others. The Chambon and Winter model defines the gel time as the point at which the storage and loss moduli follow the same power-law behaviour with respect to frequency:

$$G'(\omega) \propto G''(\omega) \propto \omega^n \quad (12)$$

This condition can be easily detected by the time or temperature at which $\tan\delta = G''/G'$ is independent of frequency, as reported in Fig. 5b. In this Fig. 5b, the behaviour of a collagen gel formed at 20 °C are presented. Based on the Winter and Chambon criterion, the material initially behaves as a liquid viscoelastic material. During this stage, the value of $\tan\delta$ decreases with increasing frequency, indicating a predominantly liquid-like behaviour. As the gelation process progresses and the three-dimensional network begins to form, the material reaches the gel point. This is characterized by $\tan\delta$ becoming frequency-independent, which occurs at approximately 280 seconds. At this stage, the gel has started to transition from a liquid-like state to a more solid-like state. After the gel point, the material behaves as a solid viscoelastic material, with $\tan\delta$ increasing with frequency.

In addition, for many tissue engineering applications involving the encapsulation of cells within a hydrogel network, it may be important to employ metrics to describe the dynamic cross-linking reactions to balance considerations regarding cross-linking kinetics, together with the final network architecture. Therefore, the gelation process can be detailed by analyzing frequency sweeps at different times, starting from the onset of crosslinking, which allows for an in-depth understanding of the microstructural evolution of the hydrogel as the crosslink density increases.

In summary, dynamic moduli $G'(\omega)$ and $G''(\omega)$, along with the transient relaxation modulus, $G(t)$ and creep compliance $J(t)$, measured within the linear viscoelastic (LVE) regime – where the material's structure is not permanently deformed and the response is independent of the applied strain amplitude – provide fundamental information about the intrinsic viscoelastic behaviour of the material. This information is crucial for predicting performance under more complex conditions.[50] The application of Maxwell models (classical and generalized models) enables the quantification of relaxation times, that is, the time needed for the material to relax, which are typically linked to the material's internal structural characteristics.[67–70]

While 3D printing processes such as extrusion-based or inkjet-based printing often involve large deformations and high shear rates—conditions that extended beyond the LVE region—the insights gained from LVE measurements remain valuable. As an example, the relaxation time and Newtonian viscosity are critical parameters to define the capillary thinning and jetting of Newtonian and viscoelastic fluids.[52] More broadly, LVE data offer a baseline for interpreting material behavior under nonlinear conditions, as discussed in Section 3.2 (non-linear rheology). A material with a broad relaxation spectrum, encompassing both fast and slow modes, can facilitate smooth flow during extrusion while enabling solid-like recovery post-deposition—key for maintaining printed shape. In creep tests, delayed recovery or permanent deformation indicates weak print fidelity, whereas immediate or partial recovery suggests enhanced structural stability.

3.2. Non-linear rheology

As already seen, the printing process requires a certain fluidity of the hydrogels under shear, while, once at rest, a self-healing structural response is needed. Due to the strong flows applied during extrusion or injection, the structure of the hydrogel is far from equilibrium and the rheological behaviour is no longer independent of the applied strain or strain rate. Therefore, the study of hydrogels under conditions closer to those of processing requires extending the evaluation from the linear regime, which explains the response of the hydrogel structure at rest, to the nonlinear regime, which governs the response during processing. The evaluation usually is discussed in terms of the non-linear rheology which involves the non-linear viscoelasticity and the non-Newtonian flow behaviour described by important flow properties such as viscosity, yield stress and thixotropy.

3.2.1. Non-linear viscoelasticity. The viscoelastic characterization of hydrogels through the well-known parameters: relaxation modulus, $G(t)$, creep compliance, $J(t)$, and dynamic moduli, G' and G'', extended to the nonlinear regime by increasing the applied strain or stress, remains of practical interest to describe the structural changes of hydrogels under large deformations. In particular, the large amplitude oscillatory shear test (LAOS) is currently high valued due to its potential sensitivity to the complex deformation mechanisms of the microstructures of hydrogels used in 3D printing. One of the most common nonlinear behaviours observed in these hydrogels is the decrease in dynamic modulus with increasing strain amplitude. This strain-softening phenomenon is usually interpreted as a loss of cross-linking and subsequent flow-induced orientation and alignment of the polymer chains. The opposite behaviour and less common increase of the dynamic modulus with strain, strain stiffening behaviour, is also reported for hydrogels, as for those composed of semi-flexible filaments, due to an intrinsic strain stiffening of the filaments.[83,84] The viscoelastic softening or fluidizing behaviour is indicative of the strain-sensitive nature of hydrogels required to be injectable or 3D printing inks. This behaviour also has beneficial implications for hydrogels designed for tissue engineering, for which stress relaxation dynamics play an important role precisely at physiologically relevant strains (10–50%). It is known that migrating or mitotic cells exert protusive forces from 0.1–10 kPa and induce strains of 10–50% depending on cell type.[85] As an example, both non-linear oscillatory strain sweeps, LAOS test, Fig. 6a, and stress relaxation testing at large strains, Fig. 6b, have been proved to be good predictors of the critical stresses for cell migration and proliferation in colloidal gelatin nanoparticle gels.[86]

However, the mathematical description of the dynamic moduli in the non-linear regime implies that eqn (7) is no longer fulfilled. There is a distinct difference in the analysis of

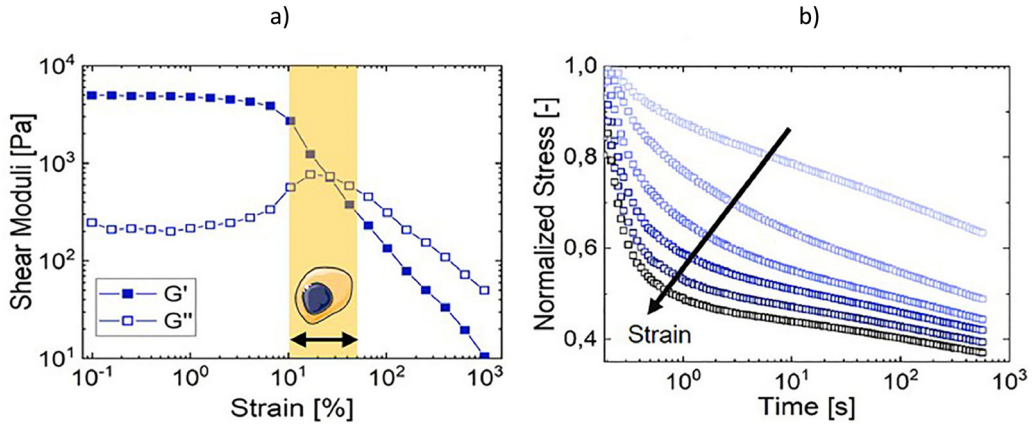

Fig. 6 Non-linear viscoelasticity: colloidal gelatin hydrogels data are adapted with permission from ref. 86. Copyright© 2021 Elsevier. (a) Linear viscoelastic regime (LVR) and non-linear (LAOS) regime with strain viscoelastic softening; (b) stress relaxations at the strain levels corresponding to those exerted by cells embedded in physiological extracellular matrices.

experimental responses, since the stress is not a perfect sinusoid and the viscoelastic moduli are no longer uniquely defined. Consequently, alternative approaches, known as LAOS (large amplitude oscillatory shear) are needed for quantifying the viscoelastic non-linear material response. The different methodologies applied to obtain relevant physical meaning from LAOS data show great potential for understanding the structural transitions that occur during 3D processing of hydrogels (gel–sol–gel) and LAOS characterization is a topic of growing interest for the 3D printing materials community.[57] For a deeper understanding of these techniques, specialized literature is recommended.[87–90]

3.2.2. Non-Newtonian behaviour. The essential parameters and settings of the printing process, such as nozzle diameter and printing pressure, determine the flow behavior of hydrogels, as will be discussed later in Section 4. The response of the material to the gradual deformation or shear applied during extrusion is primarily determined by the viscosity, which is one of the most important parameters describing the flow behaviour of hydrogels.[91] In laminar flows, a necessary condition in stable 3D printing processing, viscosity describes the internal friction between the fluid molecules. In hydrogel ink, viscosity depends on polymer concentration and chemical structure, molecular weight and morphology, as well as being sensitive to molecular interactions and shear-induced structural changes occurring during flow.[91] Viscosity requirements must be adapted to the printing technique. Inkjet printing requires very low viscosity materials (3–30 mPa s), with the low viscosity being a relevant limiting parameter as nozzle clogging is a persistent problem.[11,92] In extrusion printing, however, a wide range of hydrogel viscosities (30–10^7 mPa s) can be printed, from the low viscosities of bioprinting to avoid damage in hydrogel cell formulations, to the high viscosities that delay structural collapse when high shape fidelity is explicitly required.[93]

The materials used in 3D printing are defined by their non-Newtonian complex flow behaviour, so that they have an optimal relationship with a low viscosity during printing, and a high viscosity after deposition, behaviour that will be established depending on the different printing methods, as will be discussed below. Therefore, the viscosity evaluation must be performed under various shear flow conditions, similar to those existing during printing. To this end, it is common to measure flow through capillary and rectangular-slit dies, Couette flow through double coaxial cylinders, and steady torsional flow using parallel-plate geometry. However, an accurate characterization of the flow and deformation properties of hydrogels is challenging due to the viscoplasticity and associated slip behaviour that can affect the most relevant flow parameters. Experimental methods that avoid slip by using rough surfaces or calculations to correct for the effect of slip velocity on the flow of these viscoplastic materials are well suited procedures to ensure the determination of flow parameters and avoid erroneous information, as recently discussed in comparative studies on the viscosimetry of viscoplastic hydrogels.[94–96]

The most common non-Newtonian flow that meets the requirements for 3D printing is shear-thinning, since the apparent viscosity decreases as the shear rate increases. The most commonly models used to describe this behaviour are listed in Table 2.

The Ostwald–de Waele model (power law) is commonly used for describing the behaviour of hydrogels in the range of shear rates of the printing or injection (typically from 10^2 to 10^4 s^{-1}).[112] However, this model is a simplification of shear thinning behaviour, generally described by Carreau–Yasuda and Cross equations, including three flow regimes: Newtonian plateau at very low shear rates, power-law regime at intermediate rates, and second plateau of viscosity at high shear rates [Fig. 7a].

The Newtonian or zero shear viscosity parameter correlates with molecular characteristics, concentration, temperature, pressure and other environmental parameters (pH, physical interactions, hydrogen bonds, *etc.*). The upper viscosity, η_∞, describes the second Newtonian plateau, at the highest velocities, a region that is not accessible experimentally for the majority of the materials. The critical strain rate, $\dot{\gamma}_c$, between the Newtonian and non-Newtonian regimes characterizes the

Table 2 Models to evaluate Newtonian, pseudoplastic and viscoplastic behaviour

Newtonian	$\eta_0 = \frac{\sigma}{\dot{\gamma}}$	η_0 Newtonian viscosity σ shear stress $\dot{\gamma}$ shear rate	Newtonian liquid-assisted[97] Prepolymer solution of gelMA 5 w/w%[98]
Ostwald–de Waele or power-law	$\eta = K\dot{\gamma}^{n-1}$	η is the viscosity K is the flow consistency index n is the power law index, express the extent of shear thinning during flow η_∞ is the upper limit of the viscosity	Alginate hydrogels[99] 3D-printing of oxidized starch based hydrogels[100] Dynamically cross-linked granular hydrogels[101] Tripeptide/alginate/cellulose hydrogels[10] Alginate/gelatin hydrogels[102]
Carreau–Yasuda	$\frac{\eta-\eta_0}{\eta_0-\eta_\infty} = [1+(\lambda\dot{\gamma})^a]^{\frac{n-1}{a}}$	λ is the relaxation time, $\lambda = \frac{1}{\dot{\gamma}_c}$, where $\dot{\gamma}_c$ is the critical shear rate in the transition from newtonian to non newtonian flow a Yasuda exponent (a = 2, the equation becomes the Cross model)	Alginate solution[103] Chitosan ink[104] Chitosan/graphe oxide hydrogels[105] Gelatin methacryloyl/alginate blends without ionic crosslinking of alginate[106] GelMA-xanthan gum biomaterial ink[107]
Cross	$\eta = \eta_\infty + \frac{\eta_0-\eta_\infty}{1+(\lambda\dot{\gamma})^\alpha}$	α is related to n, and expresses the degree of shear thinning.	Carboxymethylcellulose hydrogels containing model drug[103]
Bingham	$\sigma = \sigma_y + \eta_{pl}\dot{\gamma}$	σ_y is the yield stress η_{pl} is the plastic viscosity	PVA-borax-based hydrogels[108] Gum arabic-based hidrogels[109]
Herschel–Bulkley	$\sigma = \sigma_y + K\dot{\gamma}^n$	K consistency index n extent of shear thinning	Carboxymethylcellulose hydrogels containing model drug[103] Photo-curable PVA-based hydrogel[110] Carboxymethyl cellulose-based hydrogels[40] Galic-modified hialuronic hydrogel[111]

relaxation times λ of the models. $\dot{\gamma}_c$, depends on the nature and structure of the material and is a well-defined value for homogeneous systems, whereas in many cases the transition from non-Newtonian to pseudoplastic covers a wide range of $\dot{\gamma}$. As can be seen in the Fig. 7a, the Carreau–Yasuda model best fits a fast transition type, while the Cross model accounts for a very wide transition. The index of flow, n, accounts for the slope of the curve viscosity *vs.* shear rate and expresses the degree of pseudoplasticity. A value of n close to one indicates a Newtonian behaviour, whereas n close to zero indicates pronounced shear thinning, with n = 0 being observed for plug flow, the plastic behaviour occurring before the yield stress.

3.2.3. Yield stress. The Bingham and Herschel–Bulkley models provide suitable description of yield stress fluids [Fig. 7a–c]. Upon exceeding the stress limit, the fluid can exhibit Newtonian behaviour (Bingham's model) or pseudoplastic behaviour (Herschel–Bulkley's model). The presence of a critical yield stress for the onset of flow is a relevant property of printable or injectable hydrogels. If the material is subjected to stress values below the critical yield stress, it behaves as a solid (gel), (plastic behaviour related to plug flow, n = 0), whereas if the critical limit is exceeded, the material responds with a flowing behaviour, and is sensitive to shear (sol). The yield stress property is typically associated with structured materials, such as hydrogels. When a genuine yield stress is present, the material's structure can fully recover once the shear force is removed. This behaviour is exemplified by a thermogelling nanoemulsion system evaluated below (20 °C) and above (50 °C) its gelation point, as illustrated in Fig. 8. At 20 °C (sol state), Fig. 8a displays steady shear rheology with characteristic pseudoplastic (shear-thinning) behaviour. In contrast, Fig. 8b shows the gel state at 50 °C undergoing a cyclic flow sweep—from low to high and then high to low shear rates—demonstrating a non-thixotropic, plastic response. LAOS measurements at a frequency of 20 rad s^{-1} further support these observations: the viscoelastic moduli shift under applied stresses of 500 Pa and 5 Pa indicate structure breakdown and complete recovery, respectively, confirming the presence of a true yield stress and the hydrogel's capacity for full structural regeneration.[114]

However, when the strain effects are dependent on time, thixotropy is observed, a particular behaviour that will deserve a more detailed explanation later on. In fact, the yield stress is considered to be critical factor in 3D printing extrusion-based processes. Above the yield stress the pressure required for extrusion decreases, and reversible yielding processes will correlate with the printing accuracy, mechanical stability and shape integrity of injectable/printable hydrogels.[9,50,115,116]

The stress value required to initiate flow is called the 'static yield stress' and the stress value measured when flow stops is called the 'dynamic yield stress'. In the extrusion process, the 'static yield stress' is the upper steady state limit, which indicates some structural breakage or reorganization necessary for flow to begin. Conversely, as the material exits the die and the shear rate becomes zero, the flow stops and the value of the dynamic yield stress does not relax to zero, because of the solid-elastic-like behaviour of the reformed structure. Additionally, the static and dynamic yield stress values inform about the microstructural changes that occur during printing process. Although the relationship between the static and dynamic

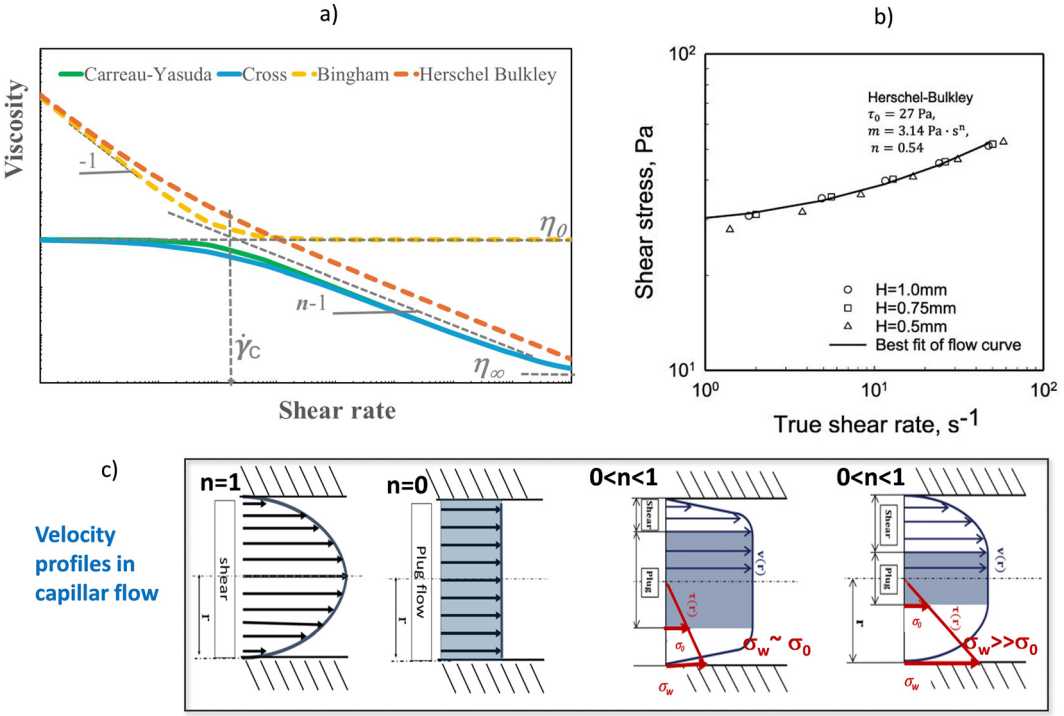

Fig. 7 Non-Newtonian flow of hydrogels: (a) pseudoplastic: Carreau–Yasuda and Cross models, and viscoplastic: Bingham and Herschel–Bulkley models (listed in Table 2), (b) yield stress from Herschel–Bulkley model with data previously corrected from slip. Data reprinted with permission from ref. 95, Copyright © 2022 MDPI. Velocity profiles in capillary flow, (c) parabolic profile of the Newtonian region (n = 1) changes to plug flow (shadow region) of viscoplastic fluids below yield stress (n = 0). Pictures adapted with permission from ref. 113 Copyright © 2019 Wiley.

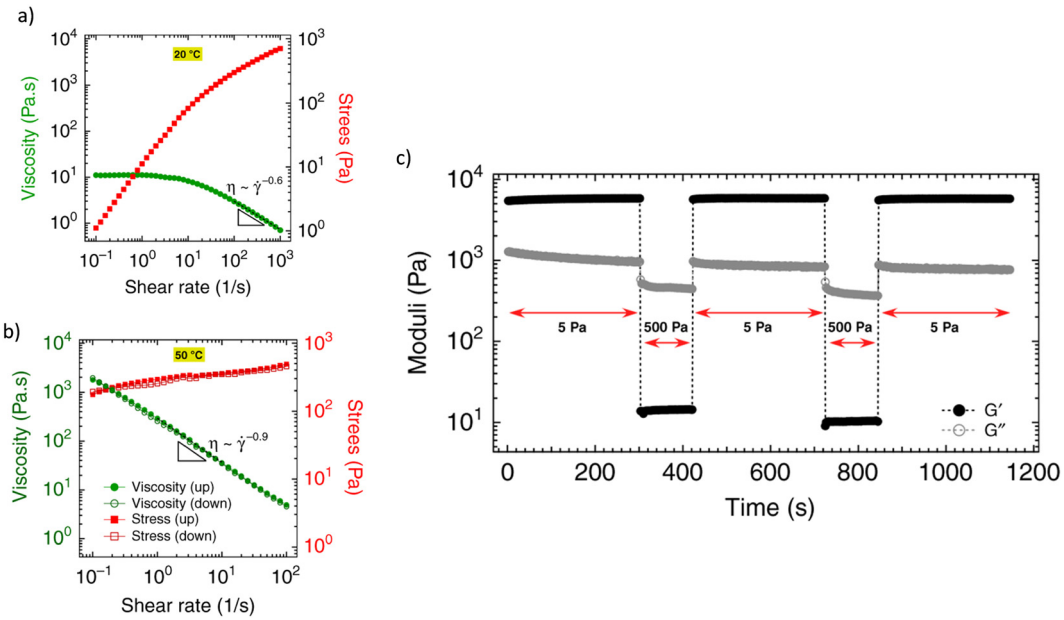

Fig. 8 Yield stress with total recovery: (a) pseudoplasticity of a thermogelling nanoemulsion below 20 °C (sol state), (b) time-independent plastic behaviour ($n \sim 0$) (gel state) above 50 °C, and, (c) total recovery of the moduli. Data reprinted with permission from ref. 114. Copyright © 2019 *Nature Comm.*

critical stress and the printability or injectability parameters are well accepted, the concept and the experimental determination of yield stresses remains one of the main rheological controversies in the rheology of soft materials. This is because most

soft materials have no real yield stress as they can flow on sufficiently long time scales. Therefore, in 3D printing, the concept of yield stress will correspond to the stress necessary for flow on the time scales relevant to the application and processing of these materials. In the practice, numerous ways are reported to determine experimentally the yield stress parameter. Reports on the field include (a) steady flow, (b) oscillatory shear, and (c) creep test, to name a few examples.[42,117,118] Fig. 7b provides an example of the determination of the yield stress for a hydrogel from steady shear flow measurements using the Herschel–Bulkley model. It should be noted that in this case, the effect of slip has been previously corrected for in order to enhance the accuracy and precision of the results.

However, to fully understand the 3D printing extrusion or injection of viscoplastic hydrogels, it is necessary to measure the flow behaviour through capillary flow experiments. Flow profiles have been studied using techniques such as embedded fluorescent bead tracking,[119,120] small-angle or neutron X-ray scattering,[121] or polarization microscopy.[122] In general, it has been shown that the flow of hydrogels exhibit a region in the centre of the capillary where there is not shear but deformation by plug flow, while near the capillary wall, the hydrogel undergoes the largest shear velocities. Fig. 7c illustrates the velocity profiles rationalized according to plastic flow models. As yield stress values is exceeded, the amplitude of the plug flow zone decreases. These results are of great relevance for hydrogels used as bioinks, as the non-sheared zone will protect cell survival.[123]

3.2.4. Thixotropy. A thixotropic fluid takes a finite time to reach equilibrium viscosity when subjected to a step change in shear rate.[124] The viscosity decreases continuously by applying a shear rate, but when the flow stops, the material start to rebuild its structure and viscosity can increase over time. Therefore, thixotropy is a time-dependent shear-thinning property related to the shear-induced structural changes. As in the case of yield stress determination, the value of thixotropy can vary depending on the specific experimental parameters of the test, so it is important to use the same experimental methods and parameters to ensure a reliable comparison between different formulations.

Thixotropy is observed usually in colloidal gels.[124,125] The microstructure of these systems changes during shearing from randomly spatially distributed particles to particles oriented with the flow direction. Upon cessation of flow, the reconstruction of the microstructure can take a long time, because only Brownian motion is present at that time. Polymer gels can also exhibit thixotropic behaviour, which is manifested by the change of their microstructure during shearing. However, the term thixotropy, in the context of hydrogel injectable design, is understood closely related to self-healing properties, as it is connected to the tendency of a gel system to reorganize the bonding interactions after the mechanical deformation. Thixotropy is understood as an optimal mechanical property observed in many gel systems where the gels break into a quasi-liquid or solution-like state under mechanical strain and recover their original form (here, gel) under static conditions. Therefore, in that context, thixotropy is a reversible, isothermal, time-dependent shear-thinning behaviour of gel systems distinguished by reversible transformation from gel–sol–gel structural transition.[126–128]

To recognize thixotropic behaviour, several measurement procedures are available. The most commonly applied is the hysteresis loop, in which a shear rate ramp-up and a consecutive ramp-down measurement are performed, until the shear rate is reduced to its initial value. If the down-ramp measurement indicates a lower viscosity and lower yield stress, thixotropy is present, and the amount of thixotropy can be deduced from the area between the hysteresis loop[125] [Fig. 9a]. Although this type of measurement is commonly used, it suffers from several shortcomings. Firstly, shear rate and time are coupled, which makes it difficult to assign the observed behaviour to the correct parameter. The second problem is the fact that the measurement is highly dependent on the shear history, the maximum shear rate and the acceleration rate. Finally, irreversible effects due to viscoelasticity can cause the formation of a

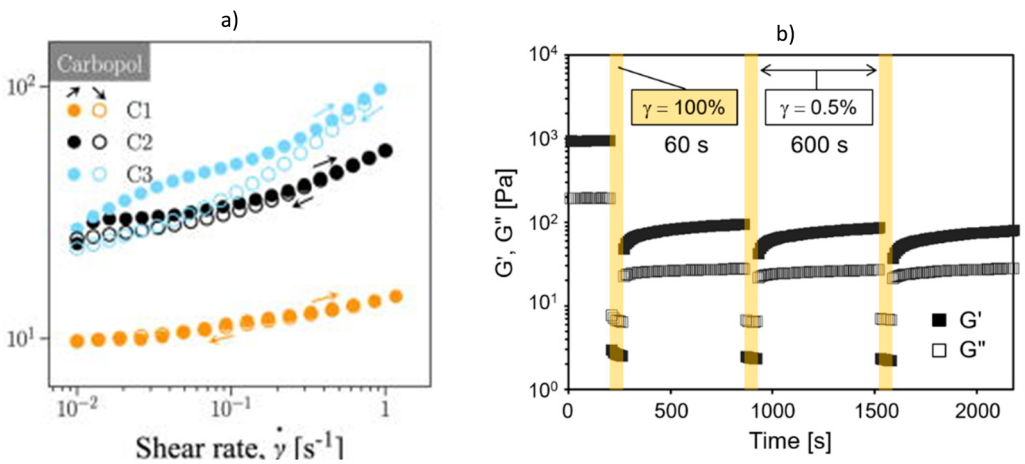

Fig. 9 Thixotropy response with finite time to structural recovery: (a) hysteresis loop for carbopol gel at different concentration. Reprinted with permission from ref. 129. Copyright© 2024 AIP Publishing, (b) irreversible structural breakdown in the experimental time scale reported for self-assembled nanofibers of double-hydrophobic elastin-like hydrogels. Reprinted with permission from ref. 126. Copyright © 2021 MDPI.

hysteresis loop, which makes it impossible to attribute the observed behaviour to the correct effects.

Another type of measurement for the determination of the thixotropy of hydrogels is the three-step oscillation method (or three-interval thixotropic test (3ITT)) [Fig. 9b]. In the experiment, three consecutive oscillation time sweeps with different strain amplitudes are applied to the sample, inside and outside the linear viscoelastic region (LVR). Thus the sequence of the experiment is as follows: (1) the structure at rest is evaluated within the LVR regime, moduli with G' higher than G'' indicates solid-type behaviour (gel state) (2) large strain amplitudes outside the linear regime cause the structure to break, and the behaviour becomes $G'' > G'$ (liquid-type behaviour), and (3) regeneration of the structure is observed at low strain amplitudes, within the LVR condition. Under LVR condition of low strain amplitude, shear does not affect the structure, thereby simulating a quiescent situation. This sequential test is employed for the assessment of thixotropic recovery. Total recovery is observed in Fig. 8c, whereas Fig. 9b shows only partial recovery, highlighting the hydrogel's thixotropic nature.

4. Bioprinting

The additive manufacturing fabrication concept has democratized the capacity for obtaining complex 3D shapes for numerous applications. One of the most important synergistic combinations is aroused by merging the intrinsic capacities of obtaining complex, multi-material three-dimensional shapes with the soft material properties provided by hydrogels, and the incorporation of biologically active components. This combination has attracted the attention of biotechnology researchers, leading to the term bioprinting.[130] As in the case of additive manufacturing, the term bioprinting does not focus on a specific type of additive manufacturing, but on the final biological application of the obtained 3D object. In the same manner, hydrogels exploited for 3D printing are known as inks or bioinks depending on their formulation. Groll *et al.* defined an ink as a biomaterial used for printing and cell-contact occurs post-fabrication, and bioink as 'a formulation of cells suitable for processing by an automated fabrication technology that may also contain biologically active components and biomaterials.[131]

Among the different bioprinting options, two major manufacturing concepts can be differentiated. The first type of manufacturing is material extrusion bioprinting.[9,132,133] This type of manufacturing focuses on the extrusion of material through a printing nozzle that selectively deposits the material to generate the final 3D part. The second type focuses on the photopolymerization of water-based precursors that give rise to the final cross-linked hydrogel.[134] In both cases, the physicochemical properties in general, and the rheological properties in particular, have imposed a series of requirements for the material to be valid in a certain type of manufacturing. Thus, the rheological characterization of the material has a pivotal role in predicting the capabilities of materials in bioprinting. In the same way, they imposed limitations for a certain types of materials, resulting in a lever for the development of new technological solutions that allow the manufacture of a greater range of materials. Thus, in the following points, the importance of rheological features in different bioprinting options will be described.

4.1. Material extrusion bioprinting

As mentioned, material extrusion bioprinting relies on the selective deposition of fluidized material through a printing nozzle or needle that, afterwards, consolidates in a solid structure capable of retaining the imposed 3D shape. The most conventional material bioprinting is the so-called direct ink writing (DIW) [Fig. 10a].

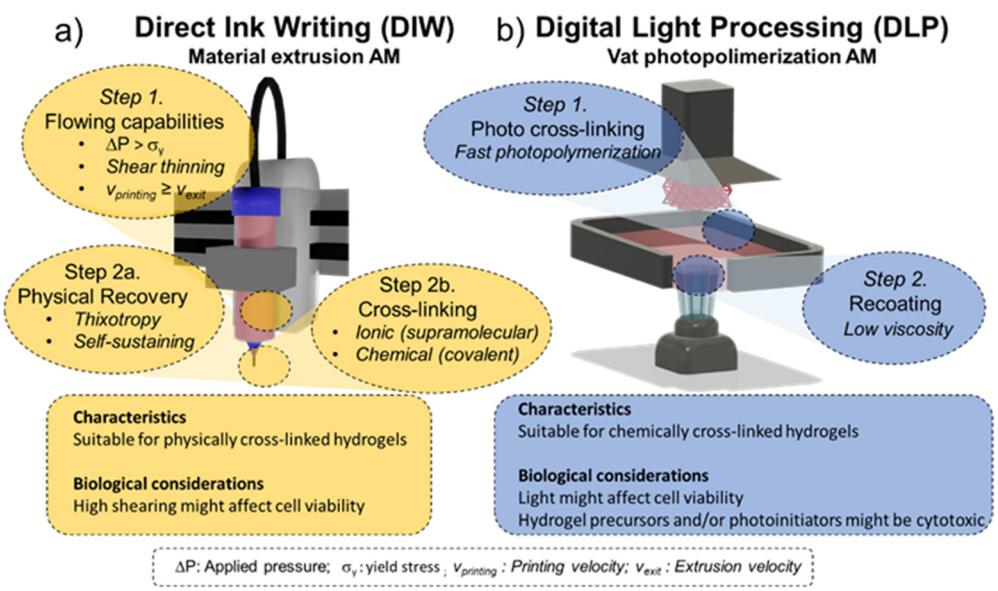

Fig. 10 Conventional bioprinting technologies: (a) direct ink writing (DIW) and (b) digital light processing (DLP).

From a rheological point of view, this process is governed by the flow capabilities of the material through the printing nozzle to produce a continuous bead. The required shear stress and the resulting shear rate can be estimated by well-established analytical equations.[72] However, these equations assume a fully-developed flow with neglectable flow entrance effects, which is usually the case. The extrusion capabilities of the material are highly affected by the geometrical configuration of the printing nozzles. Conventional printing nozzles usually present either a straight or a tapered conical configuration. In the case of straight needles, the volumetric flow (Q) can be calculated as a function of the applied pressure, as shown in eqn (13):[66]

$$Q = \frac{\pi R^3}{(1/n)+3}\left(\frac{(\Delta P)R}{2mL}\right)^{1/n} \tag{13}$$

where R and L are the capillary radius and length respectively and m and n the consistency index and pseudoplasticity index related to the power-law of pseudoplastic materials.

The analytical approximation works for tapered cylindrical geometries, resulting in eqn (14):[66]

$$\Delta P = \frac{2mL}{3n}\left[\frac{Q}{\pi}\left(\frac{1}{n}+3\right)\right]^n\left(\frac{R_L^{-3n}-R_0^{-3n}}{R_L-R_0}\right) \tag{14}$$

with R_L and R_0 as the initial and final radii of the printing needle, respectively.

During a DIW process, no material accumulation occurs and therefore, the volumetric flow that exists in the printing nozzle is deposited in the printed strand. As a first approach, it is possible to estimate the printing velocity (v_{printing}) by assuming that the printing velocity equals the exit velocity (v_{exit}) of the material. This is not always the case as (I) the printing velocity is usually higher than the exit velocity, resulting in a material elongation and (II) the layer thickness is usually lower than the nozzle diameter. However, this assumption is a good starting point for the optimization of the printing process.

After that, the material must be reconstituted to generate a solid strand capable of maintaining the printed geometry. As the main advantage of bioprinting, the obtained 3D objects tend to be porous structures produced by depositing material bridges previously printed strands. Finally, the characteristics of the ink have to provide enough mechanical support for the consecutive layers to produce the final 3D geometry. Based on these two steps, Williams *et al.* al discussed the implications of rheological parameters in DIW[55] and proposed a printability roadmap based on simple rheological experiments.[54] This initial approach might serve as a reference but is not specifically designed for hydrogels.

Extrusion-based bioprinting for hydrogels by DIW is closely connected with the yield stress and the elasticity of the fluid. As explained in Section 3, yielding fluid requires a minimum shear stress to promote the material flow. Hydrogel yield stress depends on the network structure and the presence of other components such as fillers or biologically active components (*e.g.*, cells or drugs). The effect of the material structure on the yield stress and its importance on printability in DIW printing has been recently reviewed.[2] Briefly, yield stress is related to the presence of weak interactions (*i.e.* hydrogen bonds or interparticle interactions) within the hydrogel. However, shear stresses in conventional DIW printers used to be high enough to overpass the yield stress, resulting in the material flow.

The material behaviour during flow is also considered in DIW. In fact, most of the hydrogels used for this technology showed a remarkable shear-thinning behaviour, denoted by the decrease of the viscosity as the applied shear rate increases.[59,135] As a representative example of the shear-thinning characterization, Nelson *et al.* evaluated the shear-thinning characteristic of a yielding mixture of reactive methacrylic monomers and F127-dimethacrylate hydrogels.[135] They discussed not only viscosity curves (viscosity *vs.* shear rate) but also the flow curves (stress *vs.* shear rate) and fitted the obtained results to the Hershel–Bulkley model for yielding fluids. However, multiple times shear-thinning is wrongly attributed to the hydrogel flow instead of the plug flow. Plug flow is a characteristic of the yielding fluids and it occurs when the material slips through the dye and, consequently, the inner part of the extrudate is not subjected to shear. An initial approach to identify the possible wall slip is to analyze the flow curve. A constant value of the shear stress as the shear rate increases is indicative of material slip in the measurement. This effect is translated to a characteristic slope of -1 in the viscosity curve, which can be misinterpreted as a shear-thinning behaviour. This characteristic slope of -1 does not unequivocally prove that a plug flow is generated during the extrusion of the material since the flow profiles in the rheometer and during extrusion are different, but a certain level of wall-slip should be expected.[123]

Once the material exists in the printing needle, it consolidates into a solid strand that leads to the final 3D object. This step could be approached from two different perspectives depending on the type of hydrogel printed. Many hydrogels base their printing capabilities on a physical structural recovery process (step 2a) which is usually attributed to a high thixotropic behaviour of the material, but also can be promoted by material reaction in the printing platform (*e.g.*, by UV irradiation, coagulation, or temperature change). The capacity of the hydrogel to produce a successful reconstruction after extrusion is usually addressed using a three-interval thixotropic test (3ITT).[50] As it has been commented in Section 2, this protocol consists of applying a time sweep with 3 differentiated amplitude regions. The first and last steps are performed using an amplitude within the linear viscoelastic region of the hydrogel, whereas during the middle step, a high amplitude oscillatory shear (far from the linear regime) is applied in order to simulate the flow conditions of the extrusion. The key parameter of this experiment is the time that the hydrogel requires to recover the elastic character again ($G' > G''$) after the non-linear step. In most examples of printable hydrogels, the recovery of the elastic modulus occurs almost instantly, although printable hydrogels with recoveries of up to 90 seconds have been reported.[136]

Although the previous experiments can give an idea of the capabilities of gel to be able to be printed, these results cannot be directly correlated with relevant parameters for printing

such as resolution, printing accuracy and fidelity or the maximum printing height. To address the printing capacities of materials and to correlate them with the rheological behaviour of the material, specifically designed 3D objects have been proposed as benchmark structures to correlate the ultimate printing performance and the intrinsic rheological properties of hydrogels. The maximum height that a printing can achieve is directly related to the capacity of the material to retain the shape without deforming. This characteristic is, of course, directly related to the yield stress of the material. In literature, several studies proposed an empirical threshold value for the elastic modulus between 800 and 1000 Pa.[137] However, more systematic approaches were proposed. Liu *et al.* correlated the yield stress of the printable ink with the maximum height achieved during the printing.[137] To do so, they establish the printing yield stress, σ_y^p, using a truncated cone shape as a benchmark stricter. Thus, the printing yield stress, σ_y^p, is defined as the maximum height that can be printed without observing the material buckling. Additionally, the study asses the rheological requirements for successful printing and determines that two different criteria have to be accomplished. The first one is the ''recoverability'' criterion and related to the down-ramp yield stress, σ_y^-, and the second one is to the ''material strength'' that was correlated with the creep yield stress, σ_y^{cr}, and flow yield stress, σ_f. Similarly, the maximum length of the bridges has been investigated. For that, Therriault *et al.* developed a printing protocol to address the maximum distance that a material can support without collapsing and correlated with the yield stress of the ink.[138,139]

In some cases, printed hydrogels are unable to produce three-dimensional pieces due to an inefficient consolidation process. In these cases, the material can be provided with sufficient mechanical strength through post-treatment (step 2b). The strategy consists of crosslinking the material at the nozzle exit using an external stimulus (*e.g.*, UV light, thermogelation or immersion in chemical solutions).

One of the most important aspects of printing is the fidelity and precision of the printed parts. Multiple alternatives to address printing accuracy, fidelity and precision can be found in the review papers of Marto and coworkers[91] and Malda and coworkers.[9] According to their work, the main rheological factors influencing the printing quality are the yield stress, the elastic modulus and tan delta values as well as the recovery time in thixotropic experiments. However, the quantitative analysis of the influence of each of these parameters is still unclear. According to Gillispie *et al.*,[140] G' and yield stress can be associated with the capacity to forming high bridges while high tan delta values are correlated with high turn accuracy. However, further analysis should be performed to standardize printability measurements.

4.2. Rheological restrictions for printing: beyond direct ink writing (DIW)

The rheological analysis of DIW permits the material tuning to accomplish with the printing requirements of this technology. In the same way, it imposes a series of restrictions that not all hydrogels might fulfil. In general terms, the major difficulties for a material printing can be classified into an inadequate viscosity of the material during flow and a high thixotropic effects of the ink that impede the material self-standing during printing. Researched tried to overcome these limitations and, as a result, expanded the material bioprinting beyond the conventional DIW.

4.2.1. Incorporation of rheological modifiers. Hydrogels are often formulated with rheological modifiers to achieve the appropriate rheological properties for DIW. The role of these modifiers can be to modify either the extrusion capabilities or the recovery of the hydrogel structure.

As a key parameter for extrusion, viscosity limits the printability of hydrogel materials, usually due to high viscosity. In order to produce a correct extrusion, researchers worked with rheology modifiers (usually of low molecular weight hydrogel precursors) that are crosslinked immediately after extrusion, either chemical or light-induced crosslinking.[135,141,142] Alternatively, Fitremann *et al.* proposed the printing of dimethylsulfoxide soluble low molecular weight precursors that, while printing in a water bath, are capable of producing the hydrogel through a self-assembly process.[143] However, such methodology is highly dependent on the material's self-assembly properties as well as the printing parameters. In a different approach, several researchers focus on the combination of different polymer networks to produce the required viscous dissipation for the flow. This concept of double-network proposed an interesting approach in terms of material development.[144]

However, in some cases, the viscosity has to be increased to produce a successful printing. In this case, hydrogels used to be modified with yield stress fluids (*i.e.* Carbopol or Pluronics F127) to maximize the printing capacities of such hydrogels.[145,146] These types of fluids permit as well a precise tuning of the material thixotropy and recovery after printing.

The use of rheology modifiers is highly extended in literature. However, this strategy might alter the mechanical and/or biological behaviour of the hydrogel and compromise its performance as a biomaterial. In this sense, a thorough selection of the rheological modifier is required.

4.2.2. Printing into supporting media. Obtaining objects from low-moduli gels and highly thixotropic materials presents a remarkable challenge for material printing. These types of materials attract interest as they can mimic the mechanical characteristics of extracellular matrix (ECM). However, the lack of elasticity and/or the inappropriate kinetics results in insufficient support for successive layers, resulting in the structure collapsing. In order to face these problems, new bioprinting concepts have been introduced by directly printing into supporting media.[147–149] Among other advantages, this kind of printing permits the production of vascularized objects.[147] As an example of supporting media approaches, suspended layer additive manufacturing (SLAM) takes advantage of yield stress materials of different slurries as printing media for DIW hydrogels.[149] This concept was expanded even further in order to produce embedded printing with multi-internal surfaces.[150] Undoubtedly, the rheological control of the yield stress of the

printing medium is key for successful printing in those cases. Granular hydrogels based on Carbopol ETD 2020 are considered a gold standard for yield stress supporting media[150,151] although different slurries based on agarose, gelatins[148] or Pluronic F-127[150] have also been proposed.

Another straightforward approximation was to produce the bioprinting at low temperatures. This approach was used by Forte *et al.* to produce printings of super soft hydrogel composite by directly printing into an isopropanol bath cooled using solid carbon dioxide.[152]

4.3. Vat photopolimerization bioprinting

The pioneering technology of additive manufacturing of vat photopolymerization (VP) has also been applied for hydrogel bioprinting.[134,153] The general concept behind the fabrication is the generation of a 3D object through a photoinduced chemical reaction that results in the solidification of the initial resin. Therefore, the selective illumination of the resin, either point by point or layer by layer, results in a selective solidification of the resin into the desired pattern.[19]

Initial VP relies on stereolithography (SLA) as a printing process. This fabrication consists of the irradiation of individual points of the model in a mobile printing platform. As a result of this point-by-point fabrication, high-resolution objects can be obtained, although the printing times were relatively high. Vat photopolymerization was democratized with the irruption of digital light processing (DLP). In contrast to SLA, this technology irradiates the sample layer by layer using an LED projector, which significantly reduces the price of the printing as well as the printing times. From these initial processes, new concepts arose in vat photopolymerization. The main ones are related to two-photon photopolymerization and volumetric printing. The first uses femtosecond pulses to produce photons within the reactive resin. Similarly, volumetric printing superimposes images at different angles to produce prints inside the resins without the need for printing support.

These fabrication technologies have been as well applied to hydrogel resins, leading to a new type of bioprinting technology, mainly using DLP [Fig. 10b]. In contrast to extrusion-based bioprinting, the material is not subjected to significant shear forces to produce the flow, which might eventually kill the cells and bioorganisms during printing. However, the main drawback comes from the need for application of light, which might be detrimental to cell viability, as will be discussed later.

From a material point of view, these fabrication technologies require reactive resins that, upon light irradiation, are capable of producing a solidification of the material. Similarly, hydrogel precursors have been applied to produce photocrosslinkable resins, using water as the medium that is going to be retained after polymerization.

The rheological requirements for the validation of material in vat photopolymerization are not as strict as the ones for material extrusion bioprinting. In this case, the viscosity of the resin, composed of hydrogel precursors and water, might be the most important limitation. During printing, the resin should cover the already formed layer, in order to provide fresh material for the following layer to be printed. Thus, a viscosity window is required for a correct printing, usually, between 0.1 and 10 Pa s.[154] Apart from that, rheological measurements have been extensively used for monitoring the gelation processes. The prerequisite for this type of fabrication is the material to produce a fast photopolymerization that results in the material cross-linking. The experimental condition of these tests consist of performing time sweeps while illuminating the sample. The analysis permits to follow the cross-linking kinetics, as well as determining the gelation point of the material.

4.4. Biological implications of bioprinting

The ultimate goal of bioprinting is to produce a biologically active object, where the hydrogel material, the biologically active component and the final shape interact synergistically to produce next-level applications. However, transformation processes implied in bioprinting might reduce, or even spoil, the bioactivity of the components of hydrogels.[155]

During a DIW process, material is initially subjected to relatively high shear rates (and shear stresses) that interfere the cell viability.[119,156,157] Given that cell survival depends on the velocity and shear rate profiles to which the cells are subjected, a possible approximation can be to change the velocity profile inside the printing needle. Pochan *et al.* studied the cell survival for a cell dispersion while injected through a syringe, and compared to those encapsulated within a β-haipin hydrogels.[119] They conclude that the yield stress of proposed hydrogels transforms the velocity profile of the stream into a plug flow fashion profile. This characteristic profile occurs when only the outer layers, those that are subjected to shear stresses greater than the yield stress, are able to flow. As a consequence, the cells incorporated into the core of the hydrogel do not suffer shearing forces, increasing the cell's survival. Modifying the velocity profile towards plug flow fashion profiles is an alternative that can be extrapolated to bioprinting. In fact, it is very likely that hydrogels usually named ''shear-thinning'' produce wall slip during printing. However, a correct understanding of the effect of velocity profiles on the biologically active components might permit establishing a connection between the hydrogel formulation, the rheological performance and the bioactivity of the final printing.

As mentioned, vat photopolymerization processes rely on the application of energetic lights (usually in the UV or blue range of the visible spectrum) to produce the chemical cross-linking of the hydrogel. Both the radiation itself and the chemical reaction undergoing upon irradiation have a detrimental effect on the cell survival.[158] It is widely accepted the effect of radiation in the cell viability, to the extent that the term phototoxicity was used to name this effect.[158] The adverse effect on biological structures is obviously dependent on the wavelength and dose.[134] However, the UVA range and shortwave visible wavelengths have been demonstrated harmful to cells and DNA.[159] Apart from producing soft solid 3D structures, the utilization of hydrogels can provide extra protection for cells against light and harmful environments.

Apart from radiation, multiple components of the hydrogel, such as monomers[160] or photoinitiators,[161,162] are demonstrated

cytotoxic. To overcome this problem, no cytotoxic alternatives have been developed. As a general trend, natural biopolymers or their modifications, such as gelatin-methacrylate (Gel-MA),[163] alginate[164] and others. Regarding radical photoinitiators, lithium phenyl (2,4,6-trimethyl benzoyl) phosphinate (LAP) is considered a water-soluble and non-cytotoxic gold standard photoinititator for vat photopolymerization bioprinting, although its cytotoxicity is currently under discussion.[163,165,166] As a consequence, other photoactivated cross linking chemistries are being investigated. Among them, the most promising alternative is the thiol–ene chemistry.[164,167] As an example, Burdick *et al.* developed cytocompatible norbornene-modified hyaluronic acid that were printed by DLP technology.[168] In addition, other types of photoinitiators such as conjugated polymer nanoparticles are also being explored.[169,170]

The use of hydrogels as inks for both DIW and VP bioprinting permits extra protection for bioactive molecules and cells throughout different methods. These effects, in addition to their capacity to mimic biological tissues and fulfil the rheological requirements of bioprinting, have boosted the number of applications in relevant biological and medical fields.

5. Biomedical applications of 3D/4D printed hydrogels

Advances in 3D printing technologies, along with the refinement of hydrogel features that fulfill biological functions while remaining compatible with 3D printing techniques, are driving the development of bioprinted constructs capable of more accurately replicating the morphological, biochemical, and functional characteristics of human tissues. Initially, 3D printed hydrogels must be non-cytotoxic and biocompatible for intended biomedical applications. Over the last few decades, there has also been a significant expansion in objectives, with a growing emphasis on inducing cell differentiation within 3D tissue *in vitro* models. In this regard, the hydrophilicity and swelling of hydrogels facilitate the permeation of drugs, oxygen, nutrients, metabolism, and waste for effective drug and/or cell delivery ensuring optimal cell fates for tissue repair and local microenvironment remodelling.[171] Furthermore, the ability of smart hydrogels to change their properties over time in response to external stimuli, (*i.e.*, temperature, pH, enzyme activity, or redox balance) makes 4D printed hydrogels ideal candidates for biosensing.[172]

5.1. *In vitro* tissue models

Hydrogels are used as bioinks for 3D *in vitro* models that present higher performances in comparison to traditional 2D cultures and commercial tissue-like models. For example, Lazzari *et al.* demonstrated how spheroid models of pancreatic cancer (PDAC) mimic the microenvironment's effect on drug sensitivity and treatment resistance, similar to what is seen *in vivo*. The model, which replicated key features of PDAC, was easy to use and could be valuable for drug screening, studying cancer cell-stroma interactions, and examining tumor angiogenesis.[173] Rath and co-workers developed a 3D lung cancer spheroid model with human A549 cells embedded in a collagen gel. Them, they successfully proved the efficacy of a tryptophan-rich anticancer peptide (ACP) against A549 spheroids (>75%) at low concentrations, without harming healthy human amniotic membrane mesenchymal stem cells (<15%).[174] In another study, Skardal's group designed a 3D organoid consisting of liver, cardiac, and lung constructs to investigate liver metabolism of the prodrug capecitabine into 5-fluorouracil (5-FU), thus observing downstream toxicity in lung and cardiac organoids. Furthermore, they expanded this model to six humanized constructs, including liver, cardiac, lung, endothelium, brain, and testes organoids, and demonstrated multi-tissue interactions by metabolizing the alky-lating prodrug ifosfamide in the liver organoid, which produced chloroacetaldehyde and induced downstream neurotoxicity.[175] 3D bioprinting of hydrogels affords precise control over the 3D structure and spatiotemporal distribution of materials, cells, and/or bioactive molecules. Interestingly, *in vitro* models enable the testing of novel drugs or therapies in environments that closely mimic physiological conditions, thereby avoiding animal experimentation.

In the case of 3D extrusion printing of cell-laden hydrogels, several parameters need to be considered such as the hydrogel concentration, the temperature and printing time, as well as the needle diameter and plug flow to control the shear rate facilitating the cell survival. Multiple natural and synthetic polymers have been used as hydrogel matrixes for bioinks. Alginate was one of the first types of polymeric hydrogels investigated as a bioink. Mei and co-workers synthesized biodegradable hydrogels, based on oxidized alginate modified with an arginine-glycine-aspartic acid (RGD) peptide sequence, which were used to encapsulate human adipose-derived stem cells (hADSCs) to be later printed in a defined lattice structure on a gelatin substrate that physically cross-linked the hydrogel. These alginate-based bioinks were able to modulate the proliferation and spreading of hADSCs without affecting the structure integrity of the lattice structures. The optimal parameters for hADSCs proliferation were a 5% oxidation percentage, alginate concentrations ranging from 10% to 15% w/v, and kinematic viscosities from 400 to 3000 $mm^2 s^{-1}$.[176] Primary constituents of the body's native extracellular matrix (ECM) include natural polymers like collagen, elastin, and fibrinogen, which have drawn a lot of attention in bioink formulations. In this sense, hydrogels from collagen type-I and high-G-content LF10/60 alginate with embedded preosteoblasts and hADSCs cells were also developed to promote higher osteogenic activities than the ''conventional'' alginate-based bioinks. In another approach, chondrocytes were re-suspended in collagen/alginate solutions and placed into extrusion cartridges for extrusion through a 0.26 mm V-type needle. After printing, the 3D constructs were physically crosslinked with 10% $CaCl_2$ and 0.1% FBS and incubated in the culture medium for 3, 7, and 14 days to construct *in vitro* 3D cartilage tissue. Changmo Hwang and co-workers proposed a coaxial-nozzle-based printing method using a gelatin bioink prepolymer with a tyramine functional group, containing different cell types, human umbilical vein endothelial cells (HUVECs) and human dermal

fibroblasts (HDFs), for vascular structure generation. Polyethylene glycol (PEG) was introduced as a spacer between gelatin and tyramine (GPT) to accelerate the gelation process through an enzymatic crosslinking, in less than 5 seconds. The coaxially extruded tubes, featuring HUVECs-in-core (gelatin) and HDFs-in-GPT sheath (GPT) configuration, demonstrated a radial distribution of multiple vascular cells, serving as a proof-of-concept for one-step generation of 3D vascular constructs.[177]

Nowadays, the focus is also on photopolymerizable bioinks.[178–180] Eben Alsberg and co-workers designed a photopolymerizable bioink that consisted of ionically cross-linked oxidized and methacrylate alginate (OMA) microgels. The hydrogels were easily printed to be further chemically crosslinked when a photoinitiator (PI) and a UV absorber were incorporated leading to 3D bioconstructs with a crosslinked gradient. To demonstrate their feasibility as cell-laden bioinks for 4D living cell bioprinting, three types of cells were examined, fibroblasts (NIH3T3), a cancer cell line (HeLa), and human bone marrow-derived mesenchymal stem cells (hMSCs). The cell-laden printed hydrogels showed high cellular viability after 24 h culture for 4D living cell bioprinting.[181] Khoon S. Lim *et al.* developed photocurable hydrogels based on methacrylated poly(vinyl alcohol) (PVA-MA), gelatin-methacryloyl (Gel-MA), and a visible light photoinitiator that allowed the bioprinting of constructs with high-resolution (25–50 μm). Human mesenchymal stromal cells (MSCs) and articular cartilage-derived progenitor cells (ACPCs) were laden into the hydrogels and processed through DLP 3D printing leading to bioactive constructs with long-term survival (>90%) of encapsulated cells up to 21 d.[182] In this line, Kaushik Chatterje *et al.* synthesized photocurable methacrylate-κ-carrageenan (MA-κ-CA) as a precursor for DLP 3D bioprinting with encapsulated NIH-3T3 cells, using lithium phenyl (2,4,6-trimethyl benzoyl) phosphinate (LAP) as a photoinitiator and tartrazine as a photoblocker, and exposed to the cytocompatible visible blue light (405 nm) to fabricate 3D hydrogels with complex structures. The NIH-3T3 cells embedded within the 3D printed scaffolds showed high viability and good proliferation over several days [Fig. 11A].[183]

5.2. Tissue engineering and wound healing

Natural polymer-based hydrogels have been integrated with bioactive glasses that possess angiogenic properties and aid tissue regeneration. Bertuola *et al.* fabricated 3D printed scaffolds from hydrogels formed by a mixture of natural polymers, gelatin, alginate, and hyaluronic acid, and different concentrations of bioactive glasses (2–8% wt). The hydrogels were physically crosslinked by calcium and showed tensile modulus in the range of 130 kPa to 160 kPa, similar to skin tissue. Fibroblast cells could attach and grow onto the surface of the 3D printed scaffolds, revealing they were not cytotoxic. Besides, a hydroxyapatite layer was created in the scaffolds after 2 days cell culture for osteochondral interface scaffolds.[185] Recently, we developed printable hydrogels made of alginate (Alg) pre-crosslinked with calcium, microcrystalline cellulose (MCC), and a tripeptide, Fmoc-FFY (Fmoc: 9-fluorenylmethoxycarbonyl; F: phenylalanine; Y: tyrosine), which promoted cell adhesion. The cytocompatibility of the 3D printed scaffolds was tested in contact with MG63 osteosarcoma cells. Although the cell growth was retarded in the scaffolds containing the peptide, cells exhibited a heightened propensity to foster adhesive interactions with the scaffold rather than with other cells for potential bone tissue engineering applications.[10] Silk fibroin modified with glycidyl-methacrylate (Silk-GMA) hydrogels were loaded chondrocytes and processed by DLP 3D printing. *In vitro* cell tests proved that the 3D bioprinted Silk-GMA hydrogels ensured chondrocytes viability, proliferation and differentiation to chondrogenesis. The *in vivo* transplantation of the 3D bioprinted scaffolds into a partially defected trachea rabbit model demonstrated the formation of new cartilage like tissue and epithelium surrounding the transplanted scaffolds for cartilage regeneration purposes [Fig. 11B].[184]

3D bioprinted scaffolds, with a surface of 2 × 2 cm and 400 μm thickness, were designed for cardiac tissue regeneration. They were composed of a hyaluronic acid/gelatin hydrogel matrix containing human cardiac-derived progenitor cells (hCMPCs). Subsequently, they were transplanted in a mouse model of myocardial infarction (MI) resulting in a notable decrease in adverse remodeling and the preservation of cardiac performance, as confirmed through high-resolution magnetic resonance imaging (MRI) and histological analyses. In addition, the 3D bioprinted scaffolds supported the long-term *in vivo* survival and engraftment of hCMPCs, which exhibited a progressive increase in cardiac and vascular differentiation markers over 4-weeks.[186] Tuszynski and co-workers created biomimetic central nervous system (CNS) 3D printed structures, from gelatin methacrylate (GelMA) and poly(ethylene glycol) diacrylate (PEGDA) loaded with neural progenitor cells (NPCs), which could be easily customized and scaled to match the specific shape and length of spinal cord lesions in individual patients. The 3D bioprinted scaffolds supported axon regeneration and formation of new 'neural relays' across transection sites of complete spinal cord injury *in vivo* in rodents to restore synaptic transmission and improve functional outcomes enhancing CNS regeneration.[187] In the same line, He *et al.* developed a biomimetic epithelium/stroma bilayer implant with robust surgical handling ability for corneal regeneration based on PEGDA-GelMA hydrogels *via* DLP. A bi-layer dome-shaped corneal scaffold was printed. It was comprised of a first epithelia layer formed by the rabbit corneal epithelial cells (rCECs)-laden PEGDA-GelMA hydrogel and a second fibrous stroma layer made of rabbit adipose-derived mesenchymal stem cells (rASCs)-laden PEGDA-GelMA hydrogel and orthogonally aligned. This 3D bioprinted corneal was applied in a rabbit anterior lamellar keratoplasty (ALK) model giving rise to efficient sealing of corneal defects, re-epithelialization and stromal regeneration. The synergistic interplay between the microstructure of the 3D printed corneal scaffold and the precisely positioned cells within the epithelial and stromal layers created an ideal microenvironment for corneal regeneration.[188]

5.3. Drug delivery

3D printing-based drug delivery platforms enable rapid and precise manufacturing, facilitating efficient personalized drug

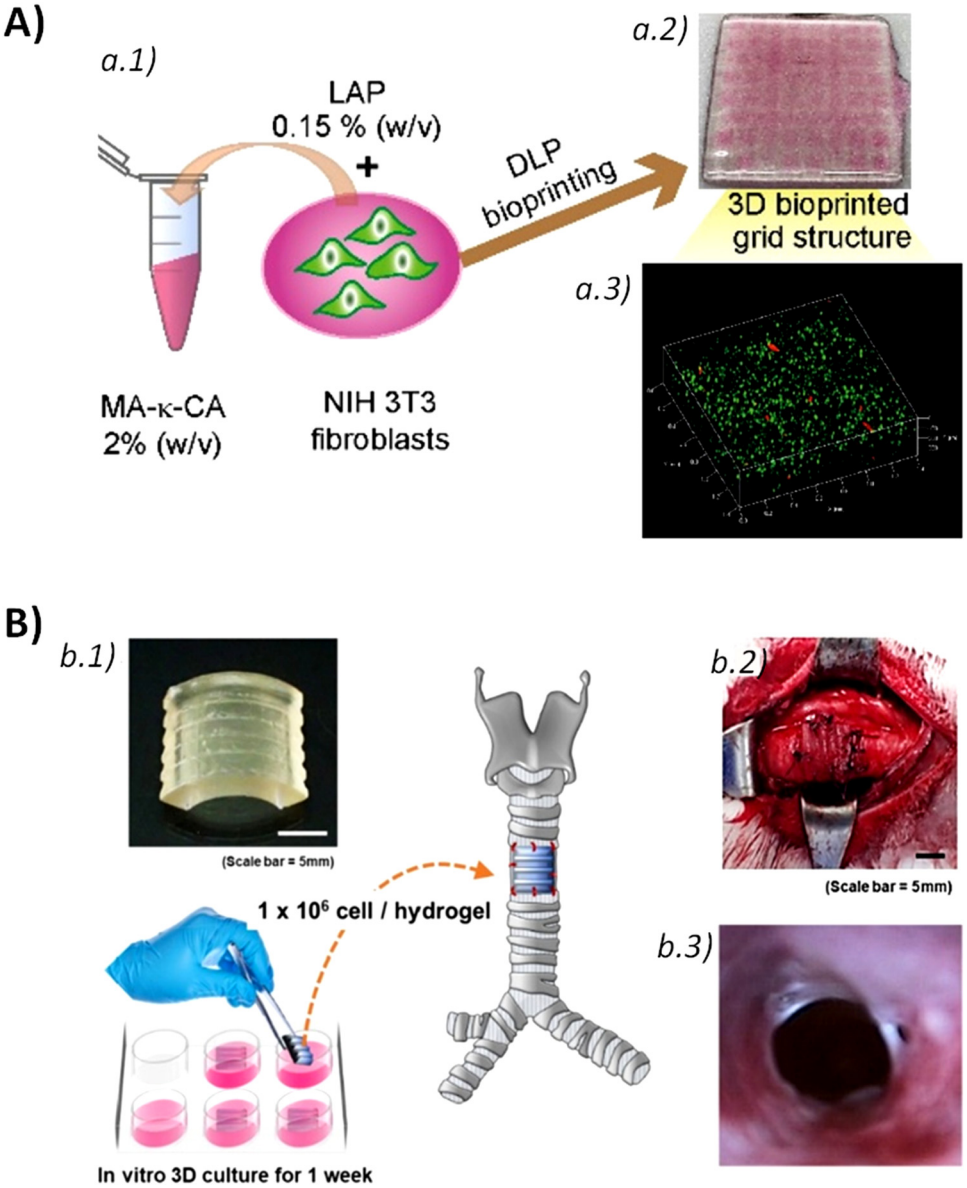

Fig. 11 (A) Schematic representation of 3D bioprinting of MA-κ-CA prepolymer solution mixed with NIH 3T3 cells (a.1) and a digital photograph of DLP printed 3D tissue construct (a.2). 3D fluorescence image of merged live/dead NIH 3T3 cells stained with calcein AM (live cells: green) and ethidium homodimer I (dead cells: red) on day 30 (a.3). Adapted and reprinted with permission from ref. 183. Copyright 2022 Elsevier. (B) Artificial trachea printed by DLP with chondrocyte from rabbit ear, and cultured for 1 week (b.1). Artificial trachea was implanted. Scale bars represent 5 mm (b.2). Endoscopy at 6 weeks after trachea transplantation (b.3). Adapted and reprinted with permission from ref. 184. Copyright 2019 Elsevier.

delivery and treatment, and minimizing the risk of side effects stemming from overdoses,[189] which is even more critical in children that need drug doses adapted to their requirements (age, weight, pathological state, *etc.*).[189,190] 3D printed patient-tailored medicinal hydrogels are a great alternative to traditional solid tablets providing an attractive and funny eye-catching appearance and rapid fabrication of dosage-personalized gummies. For such purpose, different natural polymers, including gelatin, carrageenan, xanthan gum, and starch, were investigated as hydrogel inks loaded with ranitidine hydrochloride, a drug used for the treatment of peptic ulcer disease and gastroesophageal reflux disease in children that requires a variable dosage depending on the age, weight, and clinical condition of the patient. The inks were processed by 3D extrusion printing and the printed gummy oral dosages complied with the ranitidine hydrochloride individual dose accuracy, uniformity of drug content and dissolution, which depended on the hydrogel formulation.[191] In another work, 3D printed gummies were obtained by DIW of hydrogels composed of gelatin, hydroxypropylmethyl cellulose (HPMC), reduced syrup, water, and the antiepileptic drug lamotrigine. HPMC facilitated the printing at room temperature, while the combination of gelatin and HPMC modulated the viscosity and printability of the hydrogels, and the strength of the gummy formulations after printing. Besides, the

employment of food colouring sets allowed to obtain 3D printed gummies with different colours making them more attractive for children. The drug delivery profiles of lamotrigine-loaded printed gummies showed almost 85% drug release within 15 min. They were temperature sensitive and dissolved quickly at body temperature (37 °C). Additionally, gummy formulations are generally chewed and the small pieces will result in faster drug dissolution, thus improving drug adherence of pediatric patients in future clinical settings.[192]

SLA 3D printing also allows to fabricate high-resolution unit-dose and modified-release oral dosage forms for industrial production and personalized medicine. Solid bladder devices were fabricated by SLA 3D printing of a thermoset elastic resin and lidocaine, which allowed to slow the dissolution rate of lidocaine and extend its local effect [Fig. 12A]. All solid devices (10%, 30%, and 50% drug loading) were successfully printed, with average weights of 1411.7 mg, 1564.7 mg, and 2549.2 mg, corresponding to 150 mg, 450 mg, and 1250 mg of lidocaine, respectively. The devices' outer diameters were suitable for catheter insertion. Drug delivery profiles from the 3D bladder devices were obtained in 500 mL of simulated urine fluid to simulate the dissolution conditions in the bladder. The devices with higher lidocaine content (solid 50%) showed faster release, with 90% released in 3 days. The solid 30% devices followed first-order kinetics, releasing 88% over 14 days, while the solid 10% devices had a nearly linear release, with 61% released after 14 days. Reducing the concentration of elastic resin increased the release rate due to lower crosslinking density, which enhanced drug diffusion.[193] Basit and co-workers fabricated 3D printed drug loaded hydrogels from SLA of a mixture that contained polyethylene glycol diacrylate (PEGDA), polyethylene glycol (PEG), diphenyl(2,4,6-trimethylbenzoyl)phosphine oxide as a photo-initiator, and 4-aminosalicylic acid (4-ASA) and paracetamol (acetaminophen) as model drugs. The drug loading in 3D printed hydrogels was similar to the theoretical ones, 5.69% for paracetamol and 5.40% for 4-ASA, meaning that drugs were not degraded during the 3D printing process, which is very interesting for thermally labile drugs. The dissolution profiles of the drug-loaded printed tablets were tested *in vitro* simulating gastric and intestinal conditions of the gastrointestinal tract. Results pointed out the drug release initiated in the gastric phase and persisted throughout the intestinal phase, and it was not affected by the pH. 3D printed hydrogels with different crosslinking degrees were fabricated to modulate the drug dissolution profiles by varying the percentages of PEGDA and PEG within the ink formulation. Increased quantities of PEGDA decreased the dissolution rate, whereas higher concentrations of PEG 300 facilitated the drug release. Almost 100% of paracetamol was released after 10 h from the hydrogels containing 35% PEGDA, while it decreased up to 76% for those containing 90% PEGDA. Similar trends were obtained for the 4-ASA formulations.[194] The same authors also proved the addition of water (30% w/w) to the PEGDA/PEG formulation to print hydrogels that contained and retained the water endowing them with a pre-swelling effect prior to dissolution testing, thereby increasing the drug release rate of ibuprofen.[195] In the case of polymer hydrogels to be processed by SLA, one key feature to be taken into account is the chemical reaction between the photopolymer and the drug to be loaded. Basit and co-workers showed the occurrence of a Michael addition reaction between the

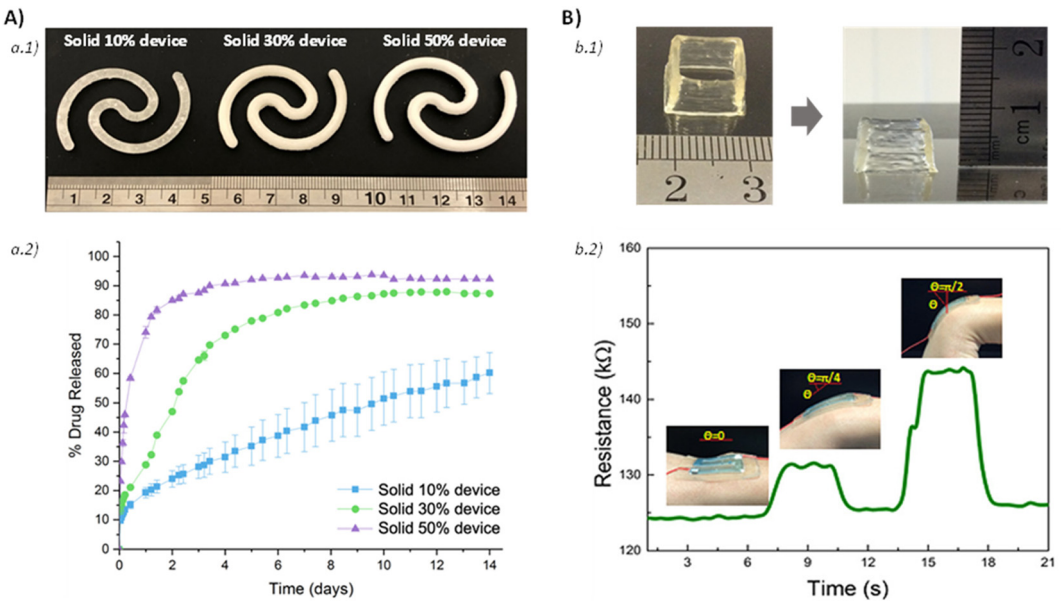

Fig. 12 (A) Photographs of the 3D printed structures, solid 10% device, solid 30% device, and solid 50% device. Scale in cm. (a.1) Cumulative release profile of lidocaine hydrochloride from the 3D printed devices (a.2). Reprinted with permission from ref. 193. Copyright 2020 Elsevier. (B) 3D printed hollow cube (left) and cone pattern (right) made of κ-carrageenan/PAAm DN hydrogel (b.1). Change of resistance with time when the 3D printed DN hydrogel with the shape of number "S" was used as a conductor, and the insets show the 3D printed DN hydrogel-based strain sensor attached on the wrist at different bending radians, 0, π/4, and π/2, respectively (b.2). Reprinted with permission from ref. 198. Copyright 2018 *Springer Nature*.

diacrylate group of PEGDA and the primary amine group of amlodipine. Therefore, a careful selection of photocurable resins needs to be addressed considering the drug to be loaded into the hydrogels to be manufactured *via* SLA 3D printing technology.[196] Very recently, Regato *et al.* developed 4D printable hydrogels from ethylene glycol/thioether acrylate (EG_nSA) monomers. The presence of acrylate groups allowed their photopolymerization by UV light, while the thioether groups conferred response to reactive oxygen species (ROS) such as H_2O_2. The flexibility of the printed hydrogels could be improved through the copolymerization of EG_3SA monomers with a polar monomer, 2-hydroxyethyl acrylate (HEA), leading to P[$(EG_3SA)_x$-*co*-HEA_y] hydrogels that were employed as matrixes for the encapsulation of a chemotherapeutic drug, 5-fluorouracil (5FU), which showed a sustained release over time modulated by the presence of H_2O_2 and the morphology of the printed scaffolds.[197]

5.4. Biosensors

Polymer hydrogels have also been used for the fabrication of flexible and wearable biosensors.[199–202] In this regard, self-healable double-network hydrogels formed by an ionically cross-linked κ-carrageenan network and a covalently cross-linked polyacrylamide (PAAm) were processed by DIW at 40–70 °C followed by an UV curing step to enhance the mechanical properties of the printed structures. They exhibited a high strain sensitivity with a gauge factor of 0.63 at 1000% strain, which allows their employment as sensitive wearable strain sensors for applications in robotics and human motion detection [Fig. 12B].[198] Wallin and collaborators developed 3D printed finger-like actuators by SLA from smart hydrogels with controlled microporosity that were able to perspire at elevated temperatures. The multimaterial fabrication required two hydrogel materials, a thermally expanding hydrogel made of PAAm to build the dermal layer, and a thermally contracting hydrogel based on poly-*n*-isopropylacrylamide (PNIPAm) for the strain-limiting actuator body at high temperatures.[203] In another work, 3D printing of PNIPAAm was carried out using projection micro-stereolithography. The temperature dependent deformation of 3D printed hydrogels depended on the polymer composition and the control of the manufacturing process parameters. Moreover, the transition temperature was also modulated through the incorporation of a hydrophilic ionic monomer, methacryl-amidopropyl-trimethyl-ammonium chloride (MAPTAC), which shifted the swelling transition temperature of PNIPAAm. These 4D printed stimuli-responsive hydrogels may be employed as flexible sensors and actuators.[204] Recently, Raquez and co-workers designed biological mimicking anisotropy-encoded hydrogel actuators made of PNIPAM and poly(2-carboxyethylacrylate) (PCEA). Gradient-like hydrogel structures were fabricated *via* SLA 3D printing by varying the crosslinking density or chemical composition of the hydrogel. The multi-responsive 4D printed hydrogel-based actuators showed rapid and reversible shape-changing ability and their bending states could be manipulated by varying the osmotic pressure (ethanol, heptane), temperature (25 and 50 °C) and pH (3 and 8).[205] Thermo- and pH-responsive hydrogels, composed of methacrylated poly(ethylene oxide)–poly(propylene oxide)–poly(ethylene oxide) (PEO–PPO–PEO) triblocks copolymerized with acrylic acid, were printed by SLA. Results demonstrated that the water uptake and dimensional changes exhibited of the 3D printed constructs depended on the temperature and pH. A fast and reversible swelling–deswelling response was observed when the pH fluctuated between 2.0 and 7.4 paving the way for the development of medical sensors.[206] Complex 4D structures consisting of acrylamide-PEGDA hydrogels covalently bonded with UV curable polymers were obtained by DLP. These hydrogels were printed mimicking cardiovascular stent morphologies to expand the blood vessel with stenosis. Their shape memory effect allowed them to be squeezed into a compacted shape at the programming temperature recovering their original shape after heating back the programming temperature.[207]

6. Conclusions and outlook

This review article focused on the rheological scientific basis of polymer hydrogels tailored for 3D and 4D printing technologies, enabling the fabrication of highly customized products that can find applications in the biomedical field. It summarized a wide variety of polymers that were used for the development of 3D printable polymer hydrogels, including synthetic polymers such as PVA, PEG, PMMA, and natural polymers like hyaluronic acid, alginate, and gelatin, among others. This wide variety of base materials, along with the different cross linking strategies – both physical (*e.g.*, hydrogen bonds, electrostatic interactions, *etc.*) and/or chemical (acrylic bonds, imine bonds, *etc.*) – significantly affects rheological properties of the hydrogels (*e.g.*, G', G'', creep compliance, yield stress, thixotropy, *etc.*), which influence their printability.

From a practical standpoint, key rheological parameters needed for additive manufacturing with hydrogels can be assessed using a torsional rheometer through basic steady or dynamic flow measurements of the initial hydrogel. First, it is necessary to study the linear rheological behaviour of the gel, that is, rheological measurements in equilibrium, to understand the structure of gels and then, the non-linear rheological behaviour, that is, rheological measurements to determine the flowability of hydrogels and their ability to recover the structure once the flow ceases. This involves characterizing shear thinning, yield stress, and thixotropic recovery as functions of applied deformation.

Nevertheless, different 3D printing technologies require distinct rheological characterizations. For material extrusion-based technologies and inkjet bioimpresion, a torsional rheometer typically provides sufficient information. In contrast, technologies such as vat photopolymerization demand photorheology experiments to monitor how the viscoelastic properties of hydrogels change under light exposure, either over time or at varying depths. Interestingly, it is noteworthy that the properties of the polymer hydrogels could be easily tuned by adjusting parameters such as the polymer(s) concentration(s), polymer mixture, crosslinking density, crosslinking type, *etc.* These modifications allow the hydrogel's properties to be

tailored to specific requirements of different printing techniques (DIW, DLP, SLA, *etc.*) and the intended application of the final printed structure. Moreover, it should be noted that the rheological properties of the polymer hydrogels are even more critical when cells are laden within the polymer bioinks during the 3D printing process to ensure a high cell viability after bioprinting.

The capacity of 3D and 4D printed polymer hydrogels to mimic the morphological, biochemical, and functional characteristics of human tissues makes them excellent candidates for different biomedical applications. These include the development of *in vitro* tissue models, tissue engineering, wound healing, drug delivery systems and biosensors. Certainly, although significant progress has been made in these areas, continued research is essential to develop nobel printable formulations with tuneable properties, enhanced biocompatibility, and stimuli-responsive behaviour (*e.g.*, temperature or pH sensitivity). Such advancements are crucial for reproduce more closely the characteristics of human tissue and organs, ultimately leading to the development of intelligent artificial organs capable of efficiently and durably replacing damaged parts of the human body and improving people's quality of life.

Current challenges in this field are guided to overcome limitations in printable hydrogel systems – for example, inadequate viscosities of the bioink during flow and a high thixotropic effect of the ink that impede the material self-standing during extrusion printing, or fast photopolymerizable resins allowing a high rate of cell survival for cell-laden bioinks.

While this review primarily focuses on biomedical applications, the potential of 3D printed polymer hydrogels extends to other innovative fields such as the food industry, soft robotics, and atmospheric water harvesting. Furthermore, advancing the study of hydrogel rheology and establishing a comprehensive database linking rheological properties to printing parameters and final material performance would represent a significant leap forward for the additive manufacturing (AM) community.

Data availability

No primary research results, software or code have been included and no new data were generated or analyzed as part of this review.

Conflicts of interest

There are no conflicts to declare.

Acknowledgements

Authors acknowledge the Spanish Ministry of Science, Innovation and Universities for financial support in the form of grant MAT 2020-83014-C2-2-P. The authors also thank the project PID2023-149734NB-C21 funded by MICIU/AEI/10.13039/501100011033 and by FEDER, UE. R. A. and I. C. acknowledges the Department of Health of the Basque Government (project 2024333015, MIRNA) for financial support. M. C.-G. thanks "Grant RYC2022-036380-I founded by MICIU/AEI/10.13039/501100011033 and FSE+" and the Emakiker program of POLYMAT (UPV/EHU).

References

1 M. Bercea, Rheology as a Tool for Fine-Tuning the Properties of Printable Bioinspired Gels, *Molecules*, 2023, **28**(6), 2766.
2 P. Wei, C. Cipriani, C. M. Hsieh, K. Kamani, S. Rogers and E. Pentzer, Go with the flow: Rheological requirements for direct ink write printability, *J. Appl. Phys.*, 2023, **134**(10), 100701.
3 G. Gillispie, P. Prim, J. Copus, J. Fisher, A. G. Mikos and J. J. Yoo, *et al.*, Assessment methodologies for extrusion-based bioink printability, *Biofabrication*, 2020, **12**(2), 022003.
4 Q. Wang, O. Backman, M. Nuopponen, C. Xu and X. Wang, Rheological and Printability Assessments on Biomaterial Inks of Nanocellulose/Photo-Crosslinkable Biopolymer in Light-Aided 3D Printing, *Front. Chem. Eng.*, 2021, **3**, 723429.
5 E. Mancha Sánchez, J. C. Gómez-Blanco, E. López Nieto, J. G. Casado, A. Macías-García and M. A. Díaz Díez, *et al.*, Hydrogels for Bioprinting: A Systematic Review of Hydrogels Synthesis, Bioprinting Parameters, and Bioprinted Structures Behavior, *Front. Bioeng. Biotechnol.*, 2020, **8**, 776.
6 L. Zhou, J. Fu and Y. He, A Review of 3D Printing Technologies for Soft Polymer Materials, *Adv. Funct. Mater.*, 2020, **30**(28), 2000187.
7 R. H. Bean, D. A. Rau, C. B. Williams and T. E. Long, Rheology guiding the design and printability of aqueous colloidal composites for additive manufacturing, *J. Vinyl Addit. Technol.*, 2023, **29**(4), 607–616.
8 J. Li, C. Wu, P. K. Chu and M. Gelinsky, 3D printing of hydrogels: Rational design strategies and emerging biomedical applications, *Mater. Sci. Eng., R*, 2020, **140**, 100543.
9 A. Schwab, R. Levato, M. D'Este, S. Piluso, D. Eglin and J. Malda, Printability and Shape Fidelity of Bioinks in 3D Bioprinting, *Chem. Rev.*, 2020, **120**(19), 11028–11055.
10 A. Hernández-Sosa, R. A. Ramírez-Jiménez, L. Rojo, F. Boulmedais, M. R. Aguilar and M. Criado-Gonzalez, *et al.*, Optimization of the Rheological Properties of Self-Assembled Tripeptide/Alginate/Cellulose Hydrogels for 3D Printing, *Polymers*, 2022, **14**(11), 2229.
11 W. L. Ng, J. M. Lee, M. Zhou, Y. W. Chen, K. X. A. Lee and W. Y. Yeong, *et al.*, Vat polymerization-based bioprinting—process, materials, applications and regulatory challenges, *Biofabrication*, 2020, **12**(2), 022001.
12 N. Ashammakhi, S. Ahadian, F. Zengjie, K. Suthiwanich, F. Lorestani and G. Orive, *et al.*, Advances and Future Perspectives in 4D Bioprinting, *Biotechnol. J.*, 2018, **13**, 1800148.
13 N. A. Chartrain, C. B. Williams and A. R. Whittington, A review on fabricating tissue scaffolds using vat photopolymerization, *Acta Biomater.*, 2018, **74**, 90–111.

14 L. Cao, L. Lu, X. Liu, J. Zhang, T. Jiang and C. Tu, *et al.*, Waiting time prediction for bottom-up vat photopolymerization, *Addit. Manuf.*, 2023, **74**, 103693.
15 W. Zhao, Z. Wang, J. Zhang, X. Wang, Y. Xu and N. Ding, *et al.*, Vat Photopolymerization 3D Printing of Advanced Soft Sensors and Actuators: From Architecture to Function, *Adv. Mater. Technol.*, 2021, **6**(8), 2001218.
16 Z. Guo, H. Zhang, W. Xie, A. Tang and W. Liu, 3D printing hydrogel with structural design *via* vat photopolymerization for strain sensing, *Addit. Manuf.*, 2023, **77**, 103824.
17 D. Baykara, T. Bedir, E. Ilhan, M. E. Mutlu, O. Gunduz and R. Narayan, *et al.*, Fabrication and optimization of 3D printed gelatin methacryloyl microneedle arrays based on vat photopolymerization, *Front. Bioeng. Biotechnol.*, 2023, **11**, 1157541.
18 O. Abdulhameed, A. Al-Ahmari, W. Ameen and S. H. Mian, Additive manufacturing: Challenges, trends, and applications, *Adv. Mech. Eng.*, 2019, **11**(2), 1687814018822880.
19 F. Zhang, L. Zhu, Z. Li, S. Wang, J. Shi and W. Tang, *et al.*, The recent development of vat photopolymerization: A review, *Addit. Manuf.*, 2021, **48**, 102423.
20 S. Chae and D. W. Cho, Biomaterial-based 3D bioprinting strategy for orthopedic tissue engineering, *Acta Biomater.*, 2023, **156**, 4–20.
21 P. Yang, Y. Ju, Y. Hu, X. Xie, B. Fang and L. Lei, Emerging 3D bioprinting applications in plastic surgery, *Biomater. Res.*, 2023, **27**(1), 1.
22 S. C. Wistner, L. Rashad and G. Slaughter, Advances in tissue engineering and biofabrication for in vitro skin modeling, *Bioprinting*, 2023, **35**, e00306.
23 A. Das, P. Awasthi, V. Jain and S. S. Banerjee, 3D printing of maxillofacial prosthesis materials: Challenges and opportunities, *Bioprinting*, 2023, **32**, e00282.
24 M. S. Chaudhry and A. Czekanski, In-situ bioprinting of skin – A review, *Bioprinting*, 2023, **31**, e00271.
25 B. Gao, Q. Yang, X. Zhao, G. Jin, Y. Ma and F. Xu, 4D Bioprinting for Biomedical Applications, *Trends Biotechnol.*, 2016, **34**(9), 746–756.
26 I. Greco, V. Miskovic, C. Varon, C. Marraffa and C. S. Iorio, Printability of Double Network Alginate-Based Hydrogel for 3D Bio-Printed Complex Structures, *Front. Bioeng. Biotechnol.*, 2022, **10**, 896166.
27 M. Criado-Gonzalez, A. Dominguez-Alfaro, N. Lopez-Larrea, N. Alegret and D. Mecerreyes, Additive Manufacturing of Conducting Polymers: Recent Advances, Challenges, and Opportunities, *ACS Appl. Polym. Mater.*, 2021, **3**(6), 2865–2883.
28 Y. W. Ding, X. W. Zhang, C. H. Mi, X. Y. Qi, J. Zhou and D. X. Wei, Recent advances in hyaluronic acid-based hydrogels for 3D bioprinting in tissue engineering applications, *Smart Mater. Med.*, 2023, **4**, 59–68.
29 S. Posniak, J. H. Y. Chung, X. Liu, P. Mukherjee and G. G. Wallace, The importance of elastin and its role in auricular cartilage tissue engineering, *Bioprinting*, 2023, **32**, e00276.
30 G. S. Irmukhametova, D. S. Kazybayeva, G. A. Mun and V. V. Khutoryanskiy, Synthesis and chemistry of hydrogels, *Hydrogels in Drug Delivery*, Elsevier, 2025, pp. 1–37.
31 B. Vigani, C. Valentino, M. Ruggeri, G. Sandri and S. Rossi, The role of hydrogels in wound healing, *Hydrogels in Drug Delivery*, Elsevier, 2025, pp. 443–476.
32 N. Zoratto and P. Matricardi, Semi-IPNs and IPN-based hydrogels, *Polymeric Gels*, Elsevier, 2018, pp. 91–124.
33 Z. Zou, B. Zhang, X. Nie, Y. Cheng, Z. Hu and M. Liao, *et al.*, A sodium alginate-based sustained-release IPN hydrogel and its applications, *RSC Adv.*, 2020, **10**(65), 39722–39730.
34 E. S. Dragan, Design and applications of interpenetrating polymer network hydrogels. A review, *Chem. Eng. J.*, 2014, **243**, 572–590.
35 C. Echeverría and C. Mijangos, Rheology Applied to Microgels: Brief (Revision of the) State of the Art, *Polymers*, 2022, **14**(7), 1279.
36 *Gels Handbook*, ed. Osada Y., Kajiwara K., Fushimi T., Irasa O., Hirokawa T., Matsunaga T., *et al.*, Elsevier, 2001.
37 G. Treloar LR, The Physics of Rubber Elasticity, 2005.
38 B. Erman and J. E. Mark, *Structures and Properties of Rubberlike Networks*, 1997.
39 G. Chaudhary, A. Ghosh, J. G. Kang, P. V. Braun, R. H. Ewoldt and K. S. Schweizer, Linear and nonlinear viscoelasticity of concentrated thermoresponsive microgel suspensions, *J. Colloid Interface Sci.*, 2021, **601**, 886–898.
40 I. Insua, O. Etzold, I. Calafel, R. Aguirresarobe, M. Calderón and M. Fernández, Rheological Insight into the 3D Printability of Carboxymethyl Cellulose-Based Hydrogels, *Gels*, 2025, **11**(4), 259.
41 G. Stojkov, Z. Niyazov, F. Picchioni and R. K. Bose, Relationship between structure and rheology of hydrogels for various applications, *Gels*, 2021, **7**(4), 255.
42 A. Z. Nelson and R. H. Ewoldt, Design of yield-stress fluids: A rheology-to-structure inverse problem, *Soft Matter*, 2017, **13**(41), 7578–7594.
43 O. Chaudhuri, J. Cooper-White, P. A. Janmey, D. J. Mooney and V. B. Shenoy, Effects of extracellular matrix viscoelasticity on cellular behaviour, *Nature*, 2020, **584**(7822), 535–546.
44 L. Ning, C. J. Gil, B. Hwang, A. S. Theus, L. Perez and M. L. Tomov, *et al.*, Biomechanical factors in three-dimensional tissue bioprinting, *Appl. Phys. Rev.*, 2020, **7**(4), 041319.
45 R. L. Truby and J. A. Lewis, Printing soft matter in three dimensions, *Nature*, 2016, **540**(7633), 371–378.
46 A. Mahajan, C. D. Frisbie and L. F. Francis, Optimization of aerosol jet printing for high-resolution, high-aspect ratio silver lines, *ACS Appl. Mater. Interfaces*, 2013, **5**(11), 4856–4864.
47 M. Fernández, M. E. Muñoz, A. Santamaría, R. Azaldegui, R. Díez and M. Peláez, Rheological analysis of highly pigmented inks: Flocculation at high temperatures, *J. Rheol.*, 1998, **42**(2), 239–253.
48 J. Li and D. J. Mooney, Designing hydrogels for controlled drug delivery, *Nat. Rev. Mater.*, 2016, **1**(12), 1–17.
49 T. C. R. Outrequin, C. Gamonpilas, W. Siriwatwechakul and P. Sreearunothai, Extrusion-based 3D printing of food

biopolymers: A highlight on the important rheological parameters to reach printability, *J. Food Eng.*, 2023, **342**, 111371.

50 P. A. Amorim, M. A. d'Ávila, R. Anand, P. Moldenaers, P. Van Puyvelde and V. Bloemen, Insights on shear rheology of inks for extrusion-based 3D bioprinting, *Bioprinting*, 2021, **22**, e00129.

51 A. Das, E. L. Gilmer, S. Biria and M. J. Bortner, Importance of Polymer Rheology on Material Extrusion Additive Manufacturing: Correlating Process Physics to Print Properties, *ACS Appl. Polym. Mater.*, 2021, **3**, 1218–1249.

52 Y. Guo, H. S. Patanwala, B. Bognet and A. W. K. Ma, Inkjet and inkjet-based 3D printing: Connecting fluid properties and printing performance, *Rapid Prototyping J.*, 2017, **23**(3), 562–576.

53 A. Corker, H. C. H. Ng, R. J. Poole and E. García-Tuñón, 3D printing with 2D colloids: Designing rheology protocols to predict ''printability'' of soft-materials, *Soft Matter*, 2019, **15**(6), 1444–1456.

54 D. A. Rau, M. J. Bortner and C. B. Williams, A rheology roadmap for evaluating the printability of material extrusion inks, *Addit. Manuf.*, 2023, **75**, 103745.

55 D. A. Rau, C. B. Williams and M. J. Bortner, Rheology and printability: A survey of critical relationships for direct ink write materials design, *Prog. Mater. Sci.*, 2023, **140**, 101188.

56 R. Agrawal and E. García-Tuñón, Interplay between yielding, 'recovery', and strength of yield stress fluids for direct ink writing: new insights from oscillatory rheology, *Soft Matter*, 2024, **20**(37), 7429–7447.

57 E. García-Tuñón, R. Agrawal, B. Ling and D. J. C. Dennis, Fourier-transform rheology and printability maps of complex fluids for three-dimensional printing, *Phys. Fluids*, 2023, **35**(1), 017113.

58 J. X. M. Chen, T. Chen, Y. Zhang, W. Fang, W. E. Li and T. Li, *et al.*, Conductive Bio-based Hydrogel for Wearable Electrodes via Direct Ink Writing on Skin, *Adv. Funct. Mater.*, 2024, **34**(40), 2403712.

59 P. Jiang, C. Yan, Y. Guo, X. Zhang, M. Cai and X. Jia, *et al.*, Direct ink writing with high-strength and swelling-resistant biocompatible physically crosslinked hydrogels, *Biomater. Sci.*, 2019, **7**(5), 1805–1814.

60 H. Herrada-Manchón, M. A. Fernández and E. Aguilar, Essential Guide to Hydrogel Rheology in Extrusion 3D Printing: How to Measure It and Why It Matters?, *Gels*, 2023, **9**(7), 517.

61 R. V. Barrulas and M. C. Corvo, Rheology in Product Development: An Insight into 3D Printing of Hydrogels and Aerogels, *Gels*, 2023, **9**(12), 986.

62 A. Skardal and A. Atala, Biomaterials for Integration with 3-D Bioprinting, *Ann. Biomed. Eng.*, 2015, **43**(3), 730–746.

63 K. Pataky, T. Braschler, A. Negro, P. Renaud, M. P. Lutolf and J. Brugger, Microdrop printing of hydrogel bioinks into 3D tissue-like geometries, *Adv. Mater.*, 2012, **24**(3), 391.

64 C. Cheng, E. J. Williamson, G. T. C. Chiu and B. Han, Engineering biomaterials by inkjet printing of hydrogels with functional particulates, *Med-X*, 2024, **2**(1), 9.

65 P. Liz-Basteiro, F. Reviriego, E. Martínez-Campos, H. Reinecke, C. Elvira and J. Rodríguez-Hernández, *et al.*, Vat Photopolymerization 3D Printing of Hydrogels with Re-Adjustable Swelling, *Gels*, 2023, **9**(8), 600.

66 R. B. Bird, R. C. Armstrong and O. Hassager, Dynamics of polymeric liquids, *Fluid mechanics*, Wiley, New York, 2nd edn, 1987, vol. 1.

67 K. Cui, Y. N. Ye, C. Yu, X. Li, T. Kurokawa and J. P. Gong, Stress Relaxation and Underlying Structure Evolution in Tough and Self-Healing Hydrogels, *ACS Macro Lett.*, 2020, **9**(11), 1582–1589.

68 S. Hafeez, A. A. Aldana, H. Duimel, F. A. A. Ruiter, M. C. Decarli and V. Lapointe, *et al.*, Molecular Tuning of a Benzene-1,3,5-Tricarboxamide Supramolecular Fibrous Hydrogel Enables Control over Viscoelasticity and Creates Tunable ECM-Mimetic Hydrogels and Bioinks, *Adv. Mater.*, 2023, **35**(24), 2207053.

69 A. M. Rosales and K. S. Anseth, The design of reversible hydrogels to capture extracellular matrix dynamics, *Nat. Rev. Mater.*, 2016, **1**(2), 1–15.

70 S. Tang, H. Ma, H. C. Tu, H. R. Wang, P. C. Lin and K. S. Anseth, Adaptable Fast Relaxing Boronate-Based Hydrogels for Probing Cell–Matrix Interactions, *Adv. Sci.*, 2018, **5**(9), 1800638.

71 J. Song, N. Holten-Andersen and G. H. McKinley, Non-Maxwellian viscoelastic stress relaxations in soft matter, *Soft Matter*, 2023, **19**(41), 7885–7906.

72 R. B. Bird, R. C. Amstrong and O. Hassager, *Dynamics of polymeric liquids*, Wiley-Interscience, 2nd edn, 1987, vol. 2.

73 D. John, *Ferry. Viscoelastic properties of polymers*, John Wiley and Sons, 1980.

74 J. Li, H. Liu, C. Wang and G. Huang, A facile method to fabricate hybrid hydrogels with mechanical toughness using a novel multifunctional cross-linker, *RSC Adv.*, 2017, **7**(56), 35311–35319.

75 S. Nam, J. Lee, D. G. Brownfield and O. Chaudhuri, Viscoplasticity Enables Mechanical Remodeling of Matrix by Cells, *Biophys. J.*, 2016, **111**(10), 2296–2308.

76 A. J. Holder, N. Badiei, K. Hawkins, C. Wright, P. R. Williams and D. J. Curtis, Control of collagen gel mechanical properties through manipulation of gelation conditions near the sol–gel transition, *Soft Matter*, 2018, **14**(4), 574–580.

77 J. M. Townsend, E. C. Beck, S. H. Gehrke, C. J. Berkland and M. S. Detamore, Flow behavior prior to crosslinking: The need for precursor rheology for placement of hydrogels in medical applications and for 3D bioprinting, *Prog. Polym. Sci.*, 2019, **91**, 126–140.

78 I. Antoniuk, D. Kaczmarek, A. Kardos, I. Varga and C. Amiel, Supramolecular Hydrogel Based on pNIPAm Microgels Connected via Host–Guest Interactions, *Polymers*, 2018, **10**(6), 566.

79 A. Garcia-Hernandez, C. Lobato-Calleros, E. J. Vernon-Carter, E. Sosa-Hernandez and J. Alvarez-Ramirez, Effects of clay concentration on the morphology and rheological properties of xanthan gum-based hydrogels reinforced

with montmorillonite particles, *J. Appl. Polym. Sci.*, 2017, **134**(8), 44517.
80 R. Lapasin, Rheological Study on Crosslinking and Gelation of Amidated Carboxymethylcellulose Solutions, *Chem. Biochem. Eng. Q.*, 2019, **32**(4), 439–449.
81 W. Hong, G. Xu, X. Ou, W. Sun, T. Wang and Z. Tong, Colloidal probe dynamics in gelatin solution during the sol–gel transition, *Soft Matter*, 2018, **14**(19), 3694–3703.
82 C. A. Bonino, J. E. Samorezov, O. Jeon, E. Alsberg and S. A. Khan, Real-time in situ rheology of alginate hydrogel photocrosslinking, *Soft Matter*, 2011, **7**(24), 11510.
83 T. De Maeseneer and R. Cardinaels, Rheological Aspects of Hydrogel Processing, *Injectable Hydrogels for 3D Bioprinting*, The Royal Society of Chemistry, 2021, pp. 238–266.
84 I. Noh, X. Wang and S. Van Vlierberghe, *Injectable hydrogels for 3D bioprinting*, Royal Society of Chemistry, 2021, vol. 8.
85 S. Nam and O. Chaudhuri, Mitotic cells generate protrusive extracellular forces to divide in three-dimensional microenvironments, *Nat. Phys.*, 2018, **14**(6), 621–628.
86 P. Bertsch, L. Andrée, N. H. Besheli and S. C. G. Leeuwenburgh, Colloidal hydrogels made of gelatin nanoparticles exhibit fast stress relaxation at strains relevant for cell activity, *Acta Biomater.*, 2022, **138**, 124–132.
87 K. Hyun, M. Wilhelm, C. O. Klein, K. S. Cho, J. G. Nam and K. H. Ahn, *et al.*, A review of nonlinear oscillatory shear tests: Analysis and application of large amplitude oscillatory shear (LAOS), *Prog. Polym. Sci.*, 2011, **36**, 1697–1753.
88 S. A. Rogers, A sequence of physical processes determined and quantified in LAOS: An instantaneous local 2D/3D approach, *J. Rheol.*, 2012, **56**(5), 1129–1151.
89 R. H. Ewoldt, A. E. Hosoi and G. H. McKinley, New measures for characterizing nonlinear viscoelasticity in large amplitude oscillatory shear, *J. Rheol.*, 2008, **52**(6), 1427–1458.
90 D. Gruis (Fred), H. Guo, D. Selinger, Q. Tian and O. A. Olsen, Surface Position, Not Signaling from Surrounding Maternal Tissues, Specifies Aleurone Epidermal Cell Fate in Maize, *Plant Physiol.*, 2006, **141**(3), 898–909.
91 S. Bom, R. Ribeiro, H. M. Ribeiro, C. Santos and J. Marto, On the progress of hydrogel-based 3D printing: Correlating rheological properties with printing behaviour, *Int. J. Pharm.*, 2022, **615**, 121506.
92 X. Li, B. Liu, B. Pei, J. Chen, D. Zhou and J. Peng, *et al.*, Inkjet Bioprinting of Biomaterials, *Chem. Rev.*, 2020, **120**(19), 10793–10833.
93 W. L. Ng, C. K. Chua and Y. F. Shen, Print Me An Organ! Why We Are Not There Yet, *Prog. Polym. Sci.*, 2019, **97**, 101145.
94 S. Aktas, D. M. Kalyon, B. M. Marín-Santibáñez and J. Pérez-González, Shear viscosity and wall slip behavior of a viscoplastic hydrogel, *J. Rheol.*, 2014, **58**(2), 513–535.
95 L. Quan and D. M. Kalyon, Parallel-Disk Viscometry of a Viscoplastic Hydrogel: Yield Stress and Other Parameters of Shear Viscosity and Wall Slip, *Gels*, 2022, **8**(4), 230.
96 B. R. Maciel, K. Baki, C. Oelschlaeger and N. Willenbacher, The Influence of Rheological and Wetting Properties of Hydrogel-based Bio-Inks on Extrusion-based Bioprinting, *Chem. Ing. Tech.*, 2022, **94**(3), 393–401.
97 R. Karyappa, D. Zhang, Q. Zhu, R. Ji, A. Suwardi and H. Liu, Newtonian liquid-assisted material extrusion 3D printing: Progress, challenges and future perspectives, *Addit. Manuf.*, 2024, **79**, 103903.
98 J. R. Xavier, T. Thakur, P. Desai, M. K. Jaiswal, N. Sears and E. Cosgriff-Hernandez, *et al.*, Bioactive nanoengineered hydrogels for bone tissue engineering: A growth-factor-free approach, *ACS Nano*, 2015, **9**(3), 3109–3118.
99 R. Sánchez-Sánchez, J. M. Rodríguez-Rego, A. Macías-García, L. Mendoza-Cerezo and A. Díaz-Parralejo, Relationship between shear-thinning rheological properties of bioinks and bioprinting parameters, *Int. J. Bioprint.*, 2023, **9**(2), 687.
100 Z. Qiu, B. Zheng, J. Xu, J. Chen and L. Chen, 3D-printing of oxidized starch-based hydrogels with superior hydration properties, *Carbohydr. Polym.*, 2022, **292**, 119686.
101 H. P. Lee, R. Davis, T. C. Wang, K. A. Deo, K. X. Cai and D. L. Alge, *et al.*, Dynamically Cross-Linked Granular Hydrogels for 3D Printing and Therapeutic Delivery, *ACS Appl. Bio Mater.*, 2023, **6**(9), 3683–3695.
102 M. P. Montes-Ballardo, J. M. Medina-Lizárraga, M. S. Flores-Jiménez and R. Q. Fuentes-Aguilar, *3D Bioprinting of Hydrogels Using Hydrophobic Sands and Calcium Chloride as Structural Support*, In: IFMBE Proceedings, 2023.
103 M. V. Ghica, M. Hîrjău, D. Lupuleasa and C. E. Dinu-Pîrvu, Flow and Thixotropic Parameters for Rheological Characterization of Hydrogels, *Molecules*, 2016, **21**(6), 786.
104 Q. Wu, D. Therriault and M. C. Heuzey, Processing and Properties of Chitosan Inks for 3D Printing of Hydrogel Microstructures, *ACS Biomater. Sci. Eng.*, 2018, **4**(7), 2643–2652.
105 J. Ahmed, M. Mulla and M. Maniruzzaman, Rheological and Dielectric Behavior of 3D-Printable Chitosan/Graphene Oxide Hydrogels, *ACS Biomater. Sci. Eng.*, 2020, **6**(1), 88–99.
106 M. Jahani Kadousaraei, S. Yamada, M. S. Aydin, A. Rashad, N. M. Cabeza and S. Mohamed-Ahmed, *et al.*, Bioprinting of mesenchymal stem cells in low concentration gelatin methacryloyl/alginate blends without ionic crosslinking of alginate, *Sci. Rep.*, 2025, **15**(1), 6609.
107 F. Iervolino, B. Belgio, A. Bonessa, F. Potere, R. Suriano and F. Boschetti, *et al.*, Versatile and non-cytotoxic GelMA-xanthan gum biomaterial ink for extrusion-based 3D bioprinting, *Bioprinting*, 2023, **31**, e00269.
108 J. Liu, Z. Yu, B. Liu, L. Liu, Y. Gao and Z. Li, *et al.*, Writable Three-Dimensional Printed Hydrogels Derived from Bingham Fluid Theory for Designable Sensors, *ACS Appl. Polym. Mater.*, 2024, **6**(16), 9420–9429.
109 T. Wang, Z. Yu, J. Si, L. Liu, X. Ren and G. Gao, Gum Arabic-based three-dimensional printed hydrogel for customizable sensors, *Int. J. Biol. Macromol.*, 2024, **254**, 128072.
110 P. Asghartabar Kashi, A. Mohammadi, J. Chen, R. Ettelaie, H. Jäger and M. Shahbazi, 3D printing of a photo-curable

hydrogel to engineer mechanically robust porous structure for ion capture or sustained potassium ferrate(VI) release for water treatment, *Sep. Purif. Technol.*, 2024, **344**, 127247.
111 K. Roshanbinfar, A. D. Evans, S. Samanta, M. Kolesnik-Gray, M. Fiedler and V. Krstic, *et al.*, Enhancing biofabrication: Shrink-resistant collagen-hyaluronan composite hydrogel for tissue engineering and 3D bioprinting applications, *Biomaterials*, 2025, **318**, 123174.
112 C. W. Macosko, *Rheology: Principles, Measurements and Applications*, Wiley-VCH, 1996.
113 S. Stieger, R. C. Kerschbaumer, E. Mitsoulis, M. Fasching, G. R. Berger-Weber and W. Friesenbichler, *et al.*, Contraction and capillary flow of a carbon black filled rubber compound, *Polym. Eng. Sci.*, 2020, **60**(1), 32–43.
114 S. M. Hashemnejad, A. Z. M. Badruddoza, B. Zarket, C. Ricardo Castaneda and P. S. Doyle, Thermoresponsive nanoemulsion-based gel synthesized through a low-energy process, *Nat. Commun.*, 2019, **10**(1), 2749.
115 M. H. Chen, L. L. Wang, J. J. Chung, Y. H. Kim, P. Atluri and J. A. Burdick, Methods To Assess Shear-Thinning Hydrogels for Application As Injectable Biomaterials, *ACS Biomater. Sci. Eng.*, 2017, **3**(12), 3146–3160.
116 S. C. Lee, G. Gillispie, P. Prim and S. J. Lee, Physical and Chemical Factors Influencing the Printability of Hydrogel-based Extrusion Bioinks, *Chem. Rev.*, 2020, **120**(19), 10834–10886.
117 A. Y. Malkin, S. R. Derkach and V. G. Kulichikhin, Rheology of Gels and Yielding Liquids, *Gels*, 2023, **9**(9), 715.
118 A. Z. Nelson, K. S. Schweizer, B. M. Rauzan, R. G. Nuzzo, J. Vermant and R. H. Ewoldt, Designing and transforming yield-stress fluids, *Curr. Opin. Solid State Mater. Sci.*, 2019, **23**(5), 100758.
119 C. Yan, M. E. Mackay, K. Czymmek, R. P. Nagarkar, J. P. Schneider and D. J. Pochan, Injectable Solid Peptide Hydrogel as a Cell Carrier: Effects of Shear Flow on Hydrogels and Cell Payload, *Langmuir*, 2012, **28**(14), 6076–6087.
120 B. D. Olsen, J. A. Kornfield and D. A. Tirrell, Yielding Behavior in Injectable Hydrogels from Telechelic Proteins, *Macromolecules*, 2010, **43**(21), 9094–9099.
121 A. Pape, M. Bastings, R. Kieltyka, H. Wyss, I. Voets and E. Meijer, *et al.*, Mesoscale Characterization of Supramolecular Transient Networks Using SAXS and Rheology, *Int. J. Mol. Sci.*, 2014, **15**(1), 1096–1111.
122 M. K. Hausmann, P. A. Rühs, G. Siqueira, J. Läuger, R. Libanori and T. Zimmermann, *et al.*, Dynamics of Cellulose Nanocrystal Alignment during 3D Printing, *ACS Nano*, 2018, **12**(7), 6926–6937.
123 P. Bertsch, M. Diba, D. J. Mooney and S. C. G. Leeuwenburgh, Self-Healing Injectable Hydrogels for Tissue Regeneration, *Chem. Rev.*, 2023, **123**(2), 834–873.
124 H. A. Barnes, Thixotropy—a review, *J. Non-Newtonian Fluid Mech.*, 1997, **70**(1–2), 1–33.
125 J. Mewis and N. J. Wagner, Thixotropy, *Adv. Colloid Interface Sci.*, 2009, **147–148**, 214–227.
126 Y. Sugioka, J. Nakamura, C. Ohtsuki and A. Sugawara-Narutaki, Thixotropic Hydrogels Composed of Self-Assembled Nanofibers of Double-Hydrophobic Elastin-Like Block Polypeptides, *Int. J. Mol. Sci.*, 2021, **22**(8), 4104.
127 B. Pramanik, Short Peptide-Based Smart Thixotropic Hydrogels, *Gels*, 2022, **8**(9), 569.
128 B. Farasati Far, M. R. Naimi-Jamal, M. Safaei, K. Zarei, M. Moradi and H. Yazdani Nezhad, A Review on Biomedical Application of Polysaccharide-Based Hydrogels with a Focus on Drug Delivery Systems, *Polymers*, 2022, **14**(24), 5432.
129 K. Amini, A. A. Mishra, A. K. Sivakumar, D. Arlov, F. Innings and R. Kádár, *et al.*, Scaling laws for near-wall flows of thixo-elasto-viscoplastic fluids in a millifluidic channel, *Phys. Fluids*, 2024, **36**(2), 023107.
130 C. Mota, S. Camarero-Espinosa, M. B. Baker, P. Wieringa and L. Moroni, Bioprinting: From Tissue and Organ Development to in Vitro Models, *Chem. Rev.*, 2020, **120**(19), 10547–10607.
131 J. Groll, J. A. Burdick, D. W. Cho, B. Derby, M. Gelinsky and S. C. Heilshorn, *et al.*, A definition of bioinks and their distinction from biomaterial inks, *Biofabrication*, 2019, **11**(1), 013001.
132 X. Cui, J. Li, Y. Hartanto, M. Durham, J. Tang and H. Zhang, *et al.*, Advances in Extrusion 3D Bioprinting: A Focus on Multicomponent Hydrogel-Based Bioinks, *Adv. Healthcare Mater.*, 2020, **9**(15), 1901648.
133 I. T. Ozbolat and M. Hospodiuk, Current advances and future perspectives in extrusion-based bioprinting, *Biomaterials*, 2016, **76**, 321–343.
134 K. S. Lim, J. H. Galarraga, X. Cui, G. C. J. Lindberg, J. A. Burdick and T. B. F. Woodfield, Fundamentals and Applications of Photo-Cross-Linking in Bioprinting, *Chem. Rev.*, 2020, **120**(19), 10662–10694.
135 P. T. Smith, A. Basu, A. Saha and A. Nelson, Chemical modification and printability of shear-thinning hydrogel inks for direct-write 3D printing, *Polymer*, 2018, **152**, 42–50.
136 N. D. Sanandiya, J. Vasudevan, R. Das, C. T. Lim and J. G. Fernandez, Stimuli-responsive injectable cellulose thixogel for cell encapsulation, *Int. J. Biol. Macromol.*, 2019, **130**, 1009–1017.
137 Y. Liu, M. Hildner, O. Roy, W. A. Van den Bogert, J. Lorenz and M. Desroches, *et al.*, On the selection of rheological tests for the prediction of 3D printability, *J. Rheol.*, 2023, **67**(4), 791.
138 K. Chizari, M. Arjmand, Z. Liu, U. Sundararaj and D. Therriault, Three-dimensional printing of highly conductive polymer nanocomposites for EMI shielding applications, *Mater. Today Commun.*, 2017, **11**, 112–118.
139 A. Habib, V. Sathish, S. Mallik and B. Khoda, 3D printability of alginate-carboxymethyl cellulose hydrogel, *Materials*, 2018, **11**(3), 454.
140 G. J. Gillispie, J. Copus, M. Uzun-Per, J. J. Yoo, A. Atala and M. K. K. Niazi, *et al.*, The correlation between rheological properties and extrusion-based printability in bioink artifact quantification, *Mater. Des.*, 2023, **233**, 112237.
141 D. Kam, A. Braner, A. Abouzglo, L. Larush, A. Chiappone and O. Shoseyov, *et al.*, 3D Printing of Cellulose

Nanocrystal-Loaded Hydrogels through Rapid Fixation by Photopolymerization, *Langmuir*, 2021, **37**(21), 6451–6458.

142 D. Petta, D. W. Grijpma, M. Alini, D. Eglin and M. D'Este, Three-Dimensional Printing of a Tyramine Hyaluronan Derivative with Double Gelation Mechanism for Independent Tuning of Shear Thinning and Postprinting Curing, *ACS Biomater. Sci. Eng.*, 2018, **4**(8), 3088–3098.

143 A. Chalard, M. Mauduit, S. Souleille, P. Joseph, L. Malaquin and J. Fitremann, 3D printing of a biocompatible low molecular weight supramolecular hydrogel by dimethylsulfoxide water solvent exchange, *Addit. Manuf.*, 2020, **33**, 101162.

144 A. A. Aldana, S. Houben, L. Moroni, M. B. Baker and L. M. Pitet, Trends in Double Networks as Bioprintable and Injectable Hydrogel Scaffolds for Tissue Regeneration, *ACS Biomater. Sci. Eng.*, 2021, **7**, 4077–4101.

145 M. Barreiro Carpio, E. Gonzalez Martinez, M. Dabaghi, J. Ungureanu, A. V. Arizpe Tafoya and D. A. Gonzalez Martinez, *et al.*, High-Fidelity Extrusion Bioprinting of Low-Printability Polymers Using Carbopol as a Rheology Modifier, *ACS Appl. Mater. Interfaces*, 2023, **15**(47), 54234–54248.

146 F. Puza, L. Barth, M. Thiel, R. Seemann and K. Lienkamp, Biocompatible, 3D Printable Magnetic Soft Actuators – Ink Formulation, Rheological Characterization and Hydrogel Actuator Prototypes, *Macromol. Mater. Eng.*, 2024, **309**(3), 2300322.

147 S. Li, J. Jin, C. Zhang, X. Yang, Y. Liu and P. Lei, *et al.*, 3D bioprinting vascular networks in suspension baths, *Appl. Mater. Today*, 2023, **30**, 101729.

148 A. M. Compaan, K. Song and Y. Huang, Gellan Fluid Gel as a Versatile Support Bath Material for Fluid Extrusion Bioprinting, *ACS Appl. Mater. Interfaces*, 2019, **11**(6), 5714–5726.

149 J. J. Senior, M. E. Cooke, L. M. Grover and A. M. Smith, Fabrication of Complex Hydrogel Structures Using Suspended Layer Additive Manufacturing (SLAM), *Adv. Funct. Mater.*, 2019, **29**(49), 1904845.

150 J. Zhao, M. Hussain, M. Wang, Z. Li and N. He, Embedded 3D printing of multi-internal surfaces of hydrogels, *Addit. Manuf.*, 2020, **32**, 101097.

151 C. S. O'Bryan, T. Bhattacharjee, S. L. Marshall, W. Gregory Sawyer and T. E. Angelini, Commercially available microgels for 3D bioprinting, *Bioprinting*, 2018, **11**, e00037.

152 Z. Tan, C. Parisi, L. Di Silvio, D. Dini and A. E. Forte, Cryogenic 3D Printing of Super Soft Hydrogels, *Sci. Rep.*, 2017, **7**(1), 16296.

153 R. Levato, O. Dudaryeva, C. E. Garciamendez-Mijares, B. E. Kirkpatrick, R. Rizzo and J. Schimelman, *et al.*, Light-based vat-polymerization bioprinting, *Nat. Rev. Methods Primers*, 2023, **3**(1), 47.

154 C. Vazquez-Martel, L. Becker, W. V. Liebig, P. Elsner and E. Blasco, Vegetable Oils as Sustainable Inks for Additive Manufacturing: A Comparative Study, *ACS Sustainable Chem. Eng.*, 2021, **9**(49), 16840–16848.

155 H. Q. Xu, J. C. Liu, Z. Y. Zhang and C. X. Xu, A review on cell damage, viability, and functionality during 3D bioprinting, *Mil. Med. Res.*, 2022, **9**(1), 70.

156 R. Chang, J. Nam and W. Sun, Effects of dispensing pressure and nozzle diameter on cell survival from solid freeform fabrication-based direct cell writing, *Tissue Eng., Part A*, 2008, **14**(1), 41–48.

157 S. Boularaoui, G. Al Hussein, K. A. Khan, N. Christoforou and C. Stefanini, An overview of extrusion-based bioprinting with a focus on induced shear stress and its effect on cell viability, *Bioprinting*, 2020, **20**, e00093.

158 C. Lee, C. D. O'Connell, C. Onofrillo, P. F. M. Choong, C. Di Bella and S. Duchi, Human articular cartilage repair: Sources and detection of cytotoxicity and genotoxicity in photo-crosslinkable hydrogel bioscaffolds, *Stem Cells Transl. Med.*, 2020, **9**(3), 302–315.

159 K. P. Lawrence, T. Douki, R. P. E. Sarkany, S. Acker, B. Herzog and A. R. Young, The UV/Visible Radiation Boundary Region (385–405 nm) Damages Skin Cells and Induces ''dark'' Cyclobutane Pyrimidine Dimers in Human Skin in vivo, *Sci. Rep.*, 2018, **8**(1), 12722.

160 M. A. Cooperstein and H. E. Canavan, Assessment of cytotoxicity of (N-isopropyl acrylamide) and poly(N-isopropyl acrylamide)-coated surfaces, *Biointerphases*, 2013, **8**(1), 19.

161 C. G. Williams, A. N. Malik, T. K. Kim, P. N. Manson and J. H. Elisseeff, Variable cytocompatibility of six cell lines with photoinitiators used for polymerizing hydrogels and cell encapsulation, *Biomaterials*, 2005, **26**(11), 1211–1218.

162 J. Huchthausen, B. I. Escher, N. Grasse, M. König, S. Beil and L. Henneberger, Reactivity of Acrylamides Causes Cytotoxicity and Activates Oxidative Stress Response, *Chem. Res. Toxicol.*, 2023, **36**(8), 1374–1385.

163 J. T. Huh, Y. W. Moon, J. Park, A. Atala, J. J. Yoo and S. J. Lee, Combinations of photoinitiator and UV absorber for cell-based digital light processing (DLP) bioprinting, *Biofabrication*, 2021, **13**(3), 034103.

164 M. Zanon, L. Montalvillo-Jiménez, R. Cue-López, E. Martínez-Campos, M. Sangermano and A. Chiappone, *et al.*, Vat 3D printing of full-alginate hydrogels via thiol-ene reactions towards tissue engineering applications, *Polym. Chem.*, 2023, **14**(42), 4856–4868.

165 A. K. Nguyen, P. L. Goering, R. K. Elespuru, S. S. Das and R. J. Narayan, The photoinitiator lithium phenyl (2,4,6-Trimethylbenzoyl) phosphinate with exposure to 405 nm light is cytotoxic to mammalian cells but not mutagenic in bacterial reverse mutation assays, *Polymers*, 2020, **12**(7), 1489.

166 A. K. Nguyen, P. L. Goering, V. Reipa and R. J. Narayan, Toxicity and photosensitizing assessment of gelatin methacryloyl-based hydrogels photoinitiated with lithium phenyl-2,4,6-trimethylbenzoylphosphinate in human primary renal proximal tubule epithelial cells, *Biointerphases*, 2019, **14**(2), 021007.

167 H. W. Ooi, C. Mota, A. Tessa Ten Cate, A. Calore, L. Moroni and M. B. Baker, Thiol-Ene Alginate Hydrogels as Versatile Bioinks for Bioprinting, *Biomacromolecules*, 2018, **19**(8), 3390–3400.

168 J. H. Galarraga, A. P. Dhand, B. P. Enzmann and J. A. Burdick, Synthesis, Characterization, and Digital Light

Processing of a Hydrolytically Degradable Hyaluronic Acid Hydrogel, *Biomacromolecules*, 2023, **24**(1), 413–425.

169 R. N. Abalos, I. A. Aziz, M. Caverzan, A. S. Lochedino, L. E. Ibarra and A. Gallastegui, *et al.*, Poly(3-hexylthiophene) nanoparticles as visible-light photoinitiators and photosensitizers in 3D printable acrylic hydrogels for photodynamic therapies, *Mater. Horiz.*, 2025, **12**(8), 2524–2534.

170 G. E. Cagnetta, A. Gallastegui, S. R. Martínez, D. Mantione, M. Criado-Gonzalez and M. Regato-Herbella, *et al.*, Conjugated Polymer Nanoparticles as Visible Light Panchromatic Photoinitiators for 3D Printing of Acrylic Hydrogels, *Macromolecules*, 2024, **57**(1), 78–87.

171 Y. Zhang and C. Wang, Recent advances in 3D printing hydrogel for topical drug delivery, *MedComm: Biomater. Appl.*, 2022, **1**(1), e211.

172 M. Tang, Q. Xie, R. C. Gimple, Z. Zhong, T. Tam and J. Tian, *et al.*, Three-dimensional bioprinted glioblastoma microenvironments model cellular dependencies and immune interactions, *Cell Res.*, 2020, **30**(10), 833–853.

173 G. Lazzari, V. Nicolas, M. Matsusaki, M. Akashi, P. Couvreur and S. Mura, Multicellular spheroid based on a triple co-culture: A novel 3D model to mimic pancreatic tumor complexity, *Acta Biomater.*, 2018, **78**, 296–307.

174 N. Dhiman, N. Shagaghi, M. Bhave, H. Sumer, P. Kingshott and S. N. Rath, Selective Cytotoxicity of a Novel Trp-Rich Peptide against Lung Tumor Spheroids Encapsulated inside a 3D Microfluidic Device, *Adv. Biosyst.*, 2020, **4**(4), 1900285.

175 S. A. P. Rajan, J. Aleman, M. M. Wan, N. Pourhabibi Zarandi, G. Nzou and S. Murphy, *et al.*, Probing prodrug metabolism and reciprocal toxicity with an integrated and humanized multi-tissue organ-on-a-chip platform, *Acta Biomater.*, 2020, **106**, 124–135.

176 J. Jia, D. J. Richards, S. Pollard, Y. Tan, J. Rodriguez and R. P. Visconti, *et al.*, Engineering alginate as bioink for bioprinting, *Acta Biomater.*, 2014, **10**(10), 4323–4331.

177 S. Hong, J. S. Kim, B. Jung, C. Won and C. Hwang, Coaxial bioprinting of cell-laden vascular constructs using a gelatin-tyramine bioink, *Biomater. Sci.*, 2019, **7**(11), 4578–4587.

178 S. B. Gugulothu, S. Asthana, S. Homer-Vanniasinkam and K. Chatterjee, Trends in Photopolymerizable Bioinks for 3D Bioprinting of Tumor Models, *JACS Au*, 2023, **3**(8), 2086–2106.

179 Z. Zhong, J. Wang, J. Tian, X. Deng, A. Balayan and Y. Sun, *et al.*, Rapid 3D bioprinting of a multicellular model recapitulating pterygium microenvironment, *Biomaterials*, 2022, **282**, 121391.

180 M. H. Kim and C. C. Lin, Poly(ethylene glycol)−Norbornene as a Photoclick Bioink for Digital Light Processing 3D Bioprinting, *ACS Appl. Mater. Interfaces*, 2023, **15**(2), 2737–2746.

181 A. Ding, O. Jeon, D. Cleveland, K. L. Gasvoda, D. Wells and S. J. Lee, *et al.*, Jammed Micro-Flake Hydrogel for Four-Dimensional Living Cell Bioprinting, *Adv. Mater.*, 2022, **34**(15), 2109394.

182 K. S. Lim, R. Levato, P. F. Costa, M. D. Castilho, C. R. Alcala-Orozco and K. M. A. Van Dorenmalen, *et al.*, Bio-resin for high resolution lithography-based biofabrication of complex cell-laden constructs, *Biofabrication*, 2018, **10**(3), 034101.

183 S. Kumari, P. Mondal and K. Chatterjee, Digital light processing-based 3D bioprinting of κ-carrageenan hydrogels for engineering cell-loaded tissue scaffolds, *Carbohydr. Polym.*, 2022, **290**, 119508.

184 H. Hong, Y. B. Seo, D. Y. Kim, J. S. Lee, Y. J. Lee and H. Lee, *et al.*, Digital light processing 3D printed silk fibroin hydrogel for cartilage tissue engineering, *Biomaterials*, 2020, **232**, 119679.

185 M. Bertuola, B. Aráoz, U. Gilabert, A. Gonzalez-Wusener, M. Pérez-Recalde and C. O. Arregui, *et al.*, Gelatin–alginate–hyaluronic acid inks for 3D printing: effects of bioglass addition on printability, rheology and scaffold tensile modulus, *J. Mater. Sci.*, 2021, **56**(27), 15327–15343.

186 R. Gaetani, D. A. M. Feyen, V. Verhage, R. Slaats, E. Messina and K. L. Christman, *et al.*, Epicardial application of cardiac progenitor cells in a 3D-printed gelatin/hyaluronic acid patch preserves cardiac function after myocardial infarction, *Biomaterials*, 2015, **61**, 339–348.

187 J. Koffler, W. Zhu, X. Qu, O. Platoshyn, J. N. Dulin and J. Brock, *et al.*, Biomimetic 3D-printed scaffolds for spinal cord injury repair, *Nat. Med.*, 2019, **25**(2), 263–269.

188 B. He, J. Wang, M. Xie, M. Xu, Y. Zhang and H. Hao, *et al.*, 3D printed biomimetic epithelium/stroma bilayer hydrogel implant for corneal regeneration, *Bioact. Mater.*, 2022, **17**, 234–247.

189 S. Mohapatra, R. K. Kar, P. K. Biswal and S. Bindhani, Approaches of 3D printing in current drug delivery, *Sens. Int.*, 2022, **3**, 100146.

190 S. A. Khaled, J. C. Burley, M. R. Alexander and C. J. Roberts, Desktop 3D printing of controlled release pharmaceutical bilayer tablets, *Int. J. Pharm.*, 2014, **461**(1–2), 105–111.

191 H. Herrada-Manchón, D. Rodríguez-González, M. Alejandro Fernández, M. Suñé-Pou, P. Pérez-Lozano and E. García-Montoya, *et al.*, 3D printed gummies: Personalized drug dosage in a safe and appealing way, *Int. J. Pharm.*, 2020, **587**, 119687.

192 T. Tagami, E. Ito, R. Kida, K. Hirose, T. Noda and T. Ozeki, 3D printing of gummy drug formulations composed of gelatin and an HPMC-based hydrogel for pediatric use, *Int. J. Pharm.*, 2021, **594**, 120118.

193 X. Xu, A. Goyanes, S. J. Trenfield, L. Diaz-Gomez, C. Alvarez-Lorenzo and S. Gaisford, *et al.*, Stereolithography (SLA) 3D printing of a bladder device for intravesical drug delivery, *Mater. Sci. Eng., C*, 2021, **120**, 111773.

194 J. Wang, A. Goyanes, S. Gaisford and A. W. Basit, Stereolithographic (SLA) 3D printing of oral modified-release dosage forms, *Int. J. Pharm.*, 2016, **503**(1–2), 207–212.

195 P. R. Martinez, A. Goyanes, A. W. Basit and S. Gaisford, Fabrication of drug-loaded hydrogels with stereolithographic 3D printing, *Int. J. Pharm.*, 2017, **532**(1), 313–317.

196 X. Xu, P. Robles-Martinez, C. M. Madla, F. Joubert, A. Goyanes and A. W. Basit, *et al.*, Stereolithography (SLA) 3D printing of an antihypertensive polyprintlet: Case

study of an unexpected photopolymer-drug reaction, *Addit. Manuf.*, 2020, **33**, 101071.

197 M. Regato-Herbella, I. Morhenn, D. Mantione, G. Pascuzzi, A. Gallastegui and A. B. Caribé dos Santos Valle, *et al.*, ROS-Responsive 4D Printable Acrylic Thioether-Based Hydrogels for Smart Drug Release, *Chem. Mater.*, 2024, **36**(3), 1262–1272.

198 S. Liu and L. Li, Ultrastretchable and Self-Healing Double-Network Hydrogel for 3D Printing and Strain Sensor, *ACS Appl. Mater. Interfaces*, 2017, **9**(31), 26429–26437.

199 S. H. Shin, W. Lee, S. M. Kim, M. Lee, J. M. Koo and S. Y. Hwang, *et al.*, Ion-conductive self-healing hydrogels based on an interpenetrating polymer network for a multimodal sensor, *Chem. Eng. J.*, 2019, **371**, 452–460.

200 L. Fan, Z. He, X. Peng, J. Xie, F. Su and D. X. Wei, *et al.*, Injectable, intrinsically antibacterial conductive hydrogels with self-healing and pH stimulus responsiveness for epidermal sensors and wound healing, *ACS Appl. Mater. Interfaces*, 2021, **13**(45), 53541–53552.

201 R. Liu, H. Wang, W. Lu, L. Cui, S. Wang and Y. Wang, *et al.*, Highly tough, stretchable and resilient hydrogels strengthened with molecular springs and their application as a wearable, flexible sensor, *Chem. Eng. J.*, 2021, **415**, 128839.

202 S. Y. Zheng, Y. Shen, F. Zhu, J. Yin, J. Qian and J. Fu, *et al.*, Programmed Deformations of 3D-Printed Tough Physical Hydrogels with High Response Speed and Large Output Force, *Adv. Funct. Mater.*, 2018, **28**(37), 1803366.

203 A. K. Mishra, W. Pan, E. P. Giannelis, R. F. Shepherd and T. J. Wallin, Making bioinspired 3D-printed autonomic perspiring hydrogel actuators, *Nat. Protoc.*, 2021, **16**(4), 2068–2087.

204 D. Han, Z. Lu, S. A. Chester and H. Lee, Micro 3D Printing of a Temperature-Responsive Hydrogel Using Projection Micro-Stereolithography, *Sci. Rep.*, 2018, **8**(1), 1963.

205 J. Odent, S. Vanderstappen, A. Toncheva, E. Pichon, T. J. Wallin and K. Wang, *et al.*, Hierarchical chemo-mechanical encoding of multi-responsive hydrogel actuators: Via 3D printing, *J. Mater. Chem. A*, 2019, **7**(25), 15395–15403.

206 S. Dutta and D. Cohn, Temperature and pH responsive 3D printed scaffolds, *J. Mater. Chem. B*, 2017, **5**(48), 9514–9521.

207 Q. Ge, Z. Chen, J. Cheng, B. Zhang, Y. F. Zhang and H. Li, *et al.*, 3D printing of highly stretchable hydrogel with diverse UV curable polymers, *Sci. Adv.*, 2021, **7**(2), eaba4261.